Clim. Past, 11, 1599–1620, 2015
www.clim-past.net/11/1599/2015/
doi:10.5194/cp-11-1599-2015

Climate of the Past
Open Access
EGU

Expansion and diversification of high-latitude radiolarian assemblages in the late Eocene linked to a cooling event in the southwest Pacific

K. M. Pascher[1,2], C. J. Hollis[1], S. M. Bohaty[3], G. Cortese[1], R. M. McKay[2], H. Seebeck[1], N. Suzuki[4], and K. Chiba[4]

[1]GNS Science, P.O. Box 30368, Lower Hutt 5040, New Zealand
[2]Victoria University Wellington, Antarctic Research Centre, P.O. Box 600, Wellington 6140, New Zealand
[3]Ocean and Earth Science, University of Southampton, National Oceanography Centre Southampton, European Way, Southampton SO14 3ZH, UK
[4]Institute of Geology and Paleontology, Graduate School of Science, Tohoku University, Sendai City, 980-8578, Japan

Correspondence to: K. M. Pascher (k.pascher@gns.cri.nz)

Received: 16 June 2015 – Published in Clim. Past Discuss.: 9 July 2015
Revised: 13 November 2015 – Accepted: 18 November 2015 – Published: 7 December 2015

Abstract. The long-term cooling trend from middle to late Eocene was punctuated by several large-scale climate perturbations that culminated in a shift to "icehouse" climates at the Eocene–Oligocene transition. We present radiolarian microfossil assemblage and foraminiferal oxygen and carbon stable isotope data from Deep Sea Drilling Project (DSDP) sites 277, 280, 281, and 283 and Ocean Drilling Project (ODP) Site 1172 to identify significant oceanographic changes in the southwest Pacific through this climate transition (∼ 40–30 Ma). We find that the Middle Eocene Climatic Optimum at ∼ 40 Ma, which is truncated but identified by a negative shift in foraminiferal δ^{18}O values at Site 277, is associated with a small increase in radiolarian taxa with low-latitude affinities (5 % of total fauna). In the early late Eocene at ∼ 37 Ma, a positive oxygen isotope shift at Site 277 is correlated with the Priabonian Oxygen Isotope Maximum (PrOM). Radiolarian abundance, diversity, and preservation increase within this cooling event at Site 277 at the same time as diatom abundance. A negative δ^{18}O excursion above the PrOM is correlated with a late Eocene warming event (∼ 36.4 Ma). Radiolarian abundance and diversity decline within this event and taxa with low-latitude affinities reappear. Apart from this short-lived warming event, the PrOM and latest Eocene radiolarian assemblages are characterised by abundant high-latitude taxa. High-latitude taxa are also abundant during the late Eocene and early Oligocene (∼ 38–30 Ma) at DSDP sites 280, 281, 283 and 1172 and are associated with very high diatom abundance. We therefore infer a northward expansion of high-latitude radiolarian taxa onto the Campbell Plateau in the latest Eocene. In the early Oligocene there is an overall decrease in radiolarian abundance and diversity at Site 277, and diatoms are scarce. These data indicate that, once the Antarctic Circumpolar Current was established in the early Oligocene (∼ 30 Ma), a frontal system similar to present day developed, with nutrient-depleted Subantarctic waters bathing the area around DSDP Site 277, resulting in a more restricted siliceous plankton assemblage.

1 Introduction

The long-term evolution of climate through the early to middle Palaeogene (56–34 Ma) has been established from geochemical proxies and palaeontological data. The primary proxy record, stable oxygen isotope (δ^{18}O) values of benthic foraminifera, shows a trend from an early Cenozoic greenhouse climate to an icehouse climate with an abrupt positive shift in benthic δ^{18}O values of ∼ 1.2–1.5 ‰ in the earliest Oligocene (∼ 34 Ma) (Shackleton and Kennett, 1975; Diester-Haass et al., 1996; Zachos et al., 2001). After a prolonged period of maximum warmth during the Early Eocene Climatic Optimum centred around 53–51 Ma, long-term cooling was interrupted by the Middle Eocene Climatic Optimum (MECO), a ∼ 500 kyr period of warmth peaking ∼ 40 Ma that has been linked to an increase in atmospheric

pCO_2 (Bohaty and Zachos, 2003; Bohaty et al., 2009; Bijl et al., 2010). Lipid biomarker-based climate proxies suggest the southwest Pacific sea surface temperatures were tropical during the MECO (28 °C) and continued to be warm throughout the late Eocene (24–26 °C), cooling only slightly across the Eocene–Oligocene transition (EOT, ∼ 22 °C) (Liu et al., 2009; Bijl et al., 2010).

The warm conditions of the Eocene indicated by geochemical proxies are generally consistent with fossil-based reconstructions of Southern Ocean circulation developed from high-latitude drill cores (Kennett, 1977; Nelson and Cooke, 2001; Kennett and Exon, 2004; Houben et al., 2013), in which subtropical waters are interpreted to have extended close to the Antarctic margin until the late Eocene. However, the latest generation of ocean circulation and climate modelling simulations fails to reproduce the degree of high-latitude warmth indicated for the Eocene by these new proxies (Hollis et al., 2012; Lunt et al., 2012). Even under hyper-greenhouse conditions, the models produce a cyclonic gyre that blocks subtropical waters from penetrating southward beyond 45° S (Huber and Sloan, 2001; Huber et al., 2004). High-latitude warmth also conflicts with increasing evidence for ephemeral Antarctic glaciation during the latest Eocene from both fossil and geochemical proxies (Lazarus and Caulet, 1993; Scher et al., 2014; Barron et al., 2015). Following the MECO event, benthic $\delta^{18}O$ values increased to their maximum Eocene values of ∼ 2.3 ‰ at about 37.3 Ma during a short-lived cooling episode in the early late Eocene, referred to as the Priabonian Oxygen Isotope Maximum (PrOM) (Scher et al., 2014). Further climate oscillations are reported for the late Eocene (Vonhof et al., 2000; Pälike et al., 2001; Bohaty and Zachos, 2003; Villa et al., 2008; Westerhold et al., 2014) prior to the expansion of Antarctic ice that defines the EOT. A negative $\delta^{18}O$ excursion reported at Ocean Drilling Project (ODP) sites 689 (Maud Rise), 738, 744, and 748 (Kerguelen Plateau) (Diester-Haass and Zahn, 1996; Bohaty and Zachos, 2003; Villa et al., 2008, 2014) has been interpreted to be a short-lived warming event in the late Eocene (∼ 36.4 Ma).

Identifying the initial timing and establishment of a high-latitude fauna in the Southern Ocean helps to constrain the development of the Southern Ocean frontal systems and, in turn, heat transfer between low and high latitudes. Kennett (1978) provided the first summary on the biogeographic development of planktic biota in the circumpolar Southern Ocean throughout the Cenozoic. He inferred that the development of distinct polar plankton assemblages was related to the evolution of the Antarctic Circumpolar Current (ACC) and the Antarctic Polar Front (AAPF). This change was linked by Kennett (1978) to Southern Ocean circulation changes associated with the opening of Drake Passage and Tasmanian Gateway in the late Eocene–early Oligocene and implicated as the main causal mechanisms for Antarctic glaciation. Subsequent deep-sea drilling campaigns have provided additional data on regional changes in Southern Ocean plankton, which were integrated by Lazarus and Caulet (1993) into a set of circumpolar maps across specific time intervals. Moreover, these authors also carried out the first synthesis of radiolarian biogeography for the region and found a pattern of increasing endemism in the Southern Ocean across the EOT. Nelson and Cooke (2001) undertook a comprehensive review of previous work and presented an updated synthesis on the oceanic front development in the southwest Pacific during the Cenozoic. According to these authors, the proto-Subtropical Front was established in the late Eocene (ca. 35 Ma) and an AAPF in the early Oligocene. A more detailed study of radiolarian biogeographic patterns and trends in the southwest Pacific was done by Lazarus et al. (2008), who found increased endemism in the radiolarian fauna in the late Eocene (ca. 35 Ma). Further radiolarian studies from the Atlantic sector of the Southern Ocean were performed by Funakawa and Nishi (2008), who recorded the first expansion of an Antarctic assemblage significantly earlier (38.5 Ma). They identified several faunal turnover events in the Antarctic assemblage from the late middle Eocene to late Oligocene and linked these events to migrations of the AAPF. Latest research suggests that the ACC was not developed until ∼ 30 Ma, together with the establishment of an AAPF (Scher et al., 2015), when the Tasmanian Gateway aligned with the westerly wind flow (Hill et al., 2013). From the middle to late Eocene, a westward Antarctic Slope Current is inferred to have flowed across the gateway, driven by the polar easterlies (Bijl et al., 2013; Scher et al., 2015).

In this paper, we document variation in radiolarian assemblages and foraminiferal oxygen and carbon stable isotopes from middle Eocene to early Oligocene (∼ 40 to 30 Ma) at Deep Sea Drilling Project (DSDP) Site 277 and relate these variations to radiolarian assemblage changes at DSDP sites 280, 281, and 283 and ODP Site 1172. DSDP Site 277 provides a unique record of pelagic sedimentation in the southwest Pacific during late Palaeocene to Oligocene times and the first Eocene foraminiferal $\delta^{18}O$ record was generated from this site (Shackleton and Kennett, 1975). Although the study by Lazarus et al. (2008) of radiolarian assemblages included all above-mentioned DSDP sites, this new work includes a more thorough taxonomic review of the radiolarian assemblages at these sites and integrates the radiolarian assemblage trends with new stable isotope data for Site 277. Our results help to identify the extent to which tropical or warm-subtropical conditions prevailed during the middle and late Eocene, refine the timing and nature of the development of a distinctive Southern Ocean radiolarian fauna and discuss implications for the palaeoceanography of the southwest Pacific from the middle Eocene to early Oligocene.

2 Study sites

Deep Sea Drilling Project (DSDP) sites 277, 280, 281 and 283 were drilled during DSDP Leg 29 (Kennett et al., 1975)

(Fig. 1). The main focus of our study is Site 277, which is located on the western margin of the Campbell Plateau (52°13.43′ S, 166°11.48′ E) at a water depth of 1214 m. Forty-six cores were drilled with a maximum penetration of 472.5 m below sea floor (mbsf), but with total length of 434.5 m of cored section and only 59.6 % recovery. Poor recovery was due to 9.5 m coring runs being conducted every 19 m (i.e. alternate drilling and coring at 9.5 m intervals) between 301.5 and 368.0 mbsf Below 10 mbsf, a Palaeogene sequence spanning from the late Palaeocene to middle Oligocene was recovered (Kennett et al., 1975). We studied cores 277-35R (349.2 mbsf) to 277-15R (134.5 mbsf), which cover a middle Eocene–lower Oligocene interval. The sediment at Site 277 (palaeolatitude ∼ 55° S) throughout the succession is highly calcareous, indicating a depositional environment well above the lysocline, with a palaeodepth estimated at around 1500 m (Kennett et al., 1975; Hollis et al., 1997).

Four additional sites were included in our study in order to acquire a regional picture of radiolarian assemblage change and biogeography during the middle Eocene to early Oligocene (Fig. 1). DSDP Site 280 comprises two holes (48°57.44′ S, 147°14.08′ E) located ∼ 100 km south of the South Tasman Rise and drilled at a water depth of 4176 m. We collected radiolarian assemblage data from Hole 280A, which consists of a 201 m cored section that includes a 97.2 m middle Eocene–middle Oligocene interval. The studied interval spans Core 280A-7R (123.4 mbsf) to Core 280A-5R (92.54 mbsf). DSDP Site 281 on the South Tasman Rise (47°59.84′ S, 147°45.85′ E), drilled at a water depth of 1591 m, encompasses two holes (281 and 281A). We examined Hole 281, which was cored to 169 mbsf, and recovered a 105.6 m (62.5 % recovery) upper Eocene–Pleistocene section. The studied interval covers cores 281-16R (149 mbsf) to 281-14R (122.5 mbsf). DSDP Site 283 lies in the central Tasman Sea (43°54.6′ S, 154°16.96′ E) at a water depth of 4729 m and also comprises two holes (283 and 283A). We examined Hole 283, which was drilled to 156 mbsf (39 % recovery), and recovered a Palaeocene–Pleistocene section that contains a hiatus from the upper Eocene to possibly the Miocene. Samples from cores 283-8R (192.25 mbsf) to 283-5R (87.75 mbsf) were studied from this site. ODP Site 1172 is situated west of the East Tasman Plateau (43°57.58′ S, 149°55.69′ E) in a water depth of 2622 m and was drilled during ODP Leg 189 (Exon et al., 2004). It comprises four holes (1172A, 1172B, 1172C and 1172D). The examined samples were from Section 1172A-39X-1 to Section 48X-CC (354.625–450.55 mbsf), spanning a middle Eocene–lower Oligocene interval, and from Section 1172D-2R-2 to Section 1172D-2R-3 (355.225–356.875 mbsf), covering a lower Oligocene interval.

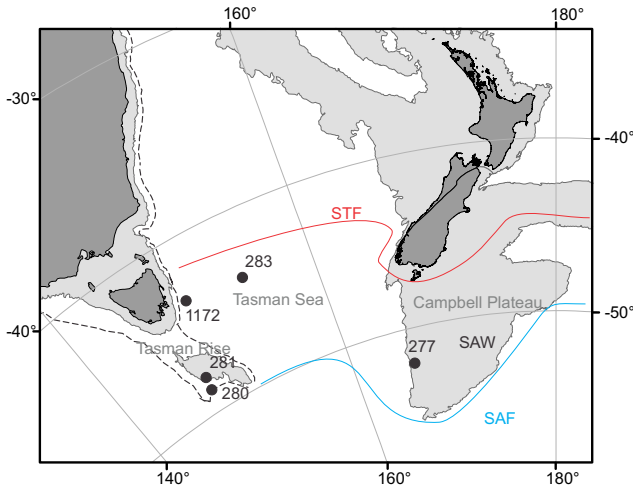

Figure 1. Modern location of DSDP and ODP study sites in the southwest Pacific. Dark grey: coastline; light grey: 2000 m isobath of continental boundary; STF: Subtropical Front; SAF: Subantarctic Front, SAW: Subantarctic Water.

3 Material and methods

3.1 Sample preparation and analysis

This study is based on 33 sediment samples from DSDP Site 277 (∼ 350 to 135 mbsf) spanning a middle Eocene–lower Oligocene interval (17 reported by Hollis et al. (1997) and 16 new samples), 6 samples from DSDP Site 283 (new, all from the DSDP/ODP Micropaleontology Reference Centre (MRC)), 7 from DSDP Site 281 (3 from the DSDP/ODP MRC, 4 new) and 4 from DSDP Site 280 (new). Due to incomplete core recovery in all study sections, the sampling resolution of our study is variable (∼ 0.5 to ∼ 30 m sample spacing). To obtain a consistent taxonomic identification across all sites, all samples previously reported from DSDP sites 277, 280, 281 and 283 were re-examined and re-counted as part of this study. The Supplement files include taxonomic notes for all radiolarian species recorded in this study, plates of selected species, and radiolarian distribution charts and sample information for DSDP sites 277, 280, 281 and 283 (Supplement Tables 1–5). Radiolarian census data of 41 samples from ODP Site 1172, covering a middle Eocene–lower Oligocene interval, are provided in Supplement Table 6. The radiolarian taxonomy, sample preparation and analysis methodology were published in Suzuki et al. (2009).

For strewn slide preparation, 1–10 g of sample material was broken into ∼ 5 mm diameter chips and acidified with 10 % HCl to dissolve carbonate. Samples were then washed through a 63 µm sieve, and the > 63 µm residue was cleaned by gently heating in a 1 : 1 solution of 10 % hydrogen peroxide and sodium hexametaphosphate ($(NaPO_3)_6$). The residue was washed through a 63 µm sieve and dried. Dependent on the volume of the processed residue and the abundance of ra-

diolarians, 1–5 strewn slides were prepared for each sample. If the radiolarians were sparse, specimens were individually picked from the dried residue under a stereo microscope. For strewn slides, a known portion of dried residue was evenly distributed on a pre-glued coverslip, which was inverted and placed gently on a glass slide with a thin coating of Canada balsam. The slide was placed on a hot plate until the balsam was fixed.

Strewn slides were examined using a Zeiss transmitted light microscope fitted with a Zeiss AxioCam ERc5s digital camera. Radiolarian census data were derived along vertical slide traverses under transmitted light following the method of Hollis (2006). For samples with sparse radiolarians (< 300 specimens per slide), all radiolarians on the prepared slide(s) were counted. For richer samples, all specimens were counted until a total number of ∼ 300 specimens was achieved. The proportion of the slide examined to this point was determined and the abundance of common taxa (> 15 observed specimens) estimated for the rest of the slide. The remaining portion was then examined and rare taxa (< 15 specimen observed in initial count) recorded. All intact tests were assigned to a counting group that range from undifferentiated order (e.g. Nassellaria undet.) and family (e.g. Actinommidae undet.) to species and subspecies. This approach allows for an accurate estimate of the abundance of individual species, but it does result in overall diversity being underestimated.

Radiolarian abundance was calculated using the following equation:

$$\left(X_{\mathrm{R}} \times X_{\mathrm{S}} \times \frac{1}{X_{\mathrm{P}}}\right) / A_{\mathrm{Sed}}, \quad (1)$$

with X_{R} being the total number of radiolarians per slide, X_{S} the number of slides made of a known portion X_{P} of the dried material, and A_{Sed} the initial amount of dried sediment.

Additional data derived for each sample assemblages includes taxic richness, the Fisher α diversity index and the Simpson index of evenness. The latter two indices were calculated using the PAST software version 3.07 (Hammer et al., 2001). The Fisher α index is a general guide to diversity, calculated from the number of taxa and the total number of individuals. The Simpson index of evenness determines the degree to which assemblages are dominated by individual taxa and ranges from 0 to 1. Since taxic richness is correlated with preservation and is also dependent on the sample size, we performed an individual rarefaction analysis for Site 277 samples with PAST (Supplement Table 2). This allows the comparison of taxonomic diversity in samples of different sizes. We used 100, 200, 300 and 500 counts as sample sizes to calculate taxic richness. Additionally, we derived a range-through taxic richness after subsampling for Site 277 with R version 3.1.3 (www.r-project.org) (Supplement Table 2). We chose sample sizes of 100 and 300, both with a subsampling of 1000. This approach shows whether a diversity drop in the middle of a series is a true diversity drop or a temporary absence due to preservation. The diatom / radiolarian (D/R) ratio was calculated using the counts of diatoms and radiolarians of one examined slide. In the case of very rare diatoms, all specimens were counted on a slide; otherwise, several transverses were counted for diatoms and the total number estimated for the whole slide. Although this method is not an accurate measure of total diatom abundance as most pelagic diatoms are smaller than the 63 µm screen used in this study, it serves to identify the order of magnitude in changes in diatom abundance that allows us to identify significant diatom event horizons.

3.2 Radiolarian biogeographic affinities

The assignment of biogeographic affinities to radiolarian species, subspecies and informally defined morphotypes encountered in our study is based on a comprehensive literature review. We focussed on published records of these taxa or their close relatives from the southwest Pacific and Southern Ocean (e.g. Petrushevskaya, 1975; Takemura and Ling, 1997; Sanfilippo and Caulet, 1998; Hollis, 2002, 2006; Funakawa and Nishi, 2005, 2008; Hollis et al., 2005; Funakawa et al., 2006; Kamikuri et al., 2013). This literature review was complemented with radiolarian occurrence data from the NSB (Neptune Sandbox Berlin) database (Lazarus, 1994; Spencer-Cervato, 1999). Unfortunately, this database lacks many Palaeogene radiolarians, and, for those that are present, occurrences need to be cross-checked with the DSDP/ODP reports. The first step was to assess the palaeolatitude of each site for the interval of radiolarian ranges. We used www.paleolatitude.org (van Hindsbergen et al., 2015) to extract palaeolatitude information in intervals of 10 Ma for the past 60 Ma and created the mean value for each site for an age range (Supplement Table 11). We listed radiolarian taxa and their range and abundance at high-latitude (> 45° N/S), mid-latitude (25–45° N/S) and low-latitude sites (0–25° N/S) and observed that presence/absence data are not always a reliable guide to biogeographic affinity (Supplement Table 12). For instance, *Lithomelissa ehrenbergi* Buetschli, 1882 was described from Barbados, which may indicate that this species has a tropical or cosmopolitan ecology. However, the species is far more abundant at high-latitude sites, and only rarely recorded at low-latitude sites. Moreover, Haeckel (1887) found recent *L. ehrenbergi* from deep-water samples at low latitudes. Therefore, we interpret this species as a cold-water indicator, commonly found in high-latitude samples and sometimes found in deep-water samples in low latitudes. The biogeographic affinities of *Amphicraspedum murrayanum* and the *A. prolixum* group also warrant some discussion. These taxa are widely reported in early and middle Eocene sediments but occur in greater abundance in the southwest Pacific at times of global warmth (Hollis, 2006). Liu et al. (2011) suggested that these taxa were not valid indicators of high-latitude warming because they are found in the Palaeocene in the North Atlantic. However, their as-

sumption that southwest Pacific and North Atlantic Ocean conditions would have been similar in the Palaeogene is not supported by ocean circulation models (Huber et al., 2003, 2004). These models indicate that oceanic conditions for the North Atlantic and the southwest Pacific were substantially different in the early Palaeogene: the North Atlantic was bathed in warm currents of ∼ 25 °C moving northwards (Huber et al., 2003), while the southwest Pacific was influenced by a strong cyclonic gyre preventing warm waters from penetrating southwards, except during times of extreme global warmth (Huber et al., 2004; Hollis et al., 2012). Thus, the occurrence of warm-water indicators throughout the Palaeocene–Eocene interval in the mid-latitude North Atlantic is consistent with both the global circulation model results and our interpretation of influxes of *Amphicraspedum* as being indicative of warming.

Tectonic reconstructions of the Australia–Antarctica–Pacific plate circuit were undertaken in GPlates version 1.5 (Boyden et al., 2011) using finite poles of rotation for the relative motions between Australia and East Antarctica from Cande and Stock (2004) (0–38.13 Ma), East Antarctica and West Antarctica from Granot et al. (2013) (30.94–40.13 Ma), and West Antarctica and the Pacific from Croon et al. (2008) (0–47.54 Ma). Relative motions of the Australia–Antarctica–Pacific plate circuit were tied to the Australian palaeomagnetic apparent polar wander path of Torsvik et al. (2012) to provide an estimate of palaeolatitude appropriate for palaeoclimate studies (van Hinsbergen et al., 2015). The 2000 m isobath from the GEBCO bathymetric grid (www.gebco.net) was used to approximate continental boundaries. The continental–oceanic boundaries of Bird (2003) are also shown (dashed lines in Figs. 1 and 8) for regions where extension has significantly thinned continental crust. Each DSDP and ODP study site was assigned to the appropriate plate for reconstruction.

The overlap of the North and South Island of New Zealand in these reconstructions is a consequence of the finite poles of rotation determined from the Adare Trough by Granot et al. (2013), which constrain the motion of East and West Antarctica between 40 and 30 Ma. These new poles result in a poor fit (significant overlap) of continental crust between the two islands that is not supported by geological data. The discrepancy between geological and palaeomagnetic data could be reconciled with the use of seafloor spreading data from the Emerald Basin (e.g. Keller, 2003), which describes Australia–Pacific relative motions (Sutherland, 1995) between 40 and 30 Ma, and the Adare Trough. However, our sites lie south of New Zealand and so we make no attempt to resolve this issue here.

3.3 Stable isotope analysis

Stable oxygen (δ^{18}O) and carbon (δ^{13}C) isotope measurements of foraminiferal samples from Site 277 were conducted in the stable isotope laboratories at the University of Southampton (UoS) and University of California Santa Cruz (UCSC). Sample analyses included bulk carbonate, benthic foraminifera (*Cibicidoides* spp.), and the planktic foraminifera *Subbotina* spp. (thermocline) from 332.62 to 159.88 mbsf and *Globigerinatheka index* (mixed layer) from 332.62 to 188.58 mbsf (its last occurrence). In total, 169 samples spanning the middle Eocene–lower Oligocene interval of DSDP Hole 277 were measured (Supplement Tables 7–10). Stable isotope analyses at the UoS were performed on a Europa GEO 20-20 dual-inlet mass spectrometer with CAPS preparation oven maintained at 70 °C, and analyses at UCSC were performed on a VG Prism dual-inlet mass spectrometer coupled to a carousel preparation device with a common acid bath maintained at 90 °C. All values are reported relative to the Vienna Pee Dee Belemnite (VPDB) standard. In both labs, analytical precision, based on replicate analyses of in-house marble standards and NBS-19, averaged ∼ 0.07 ‰ (1σ) for δ^{13}C and ∼ 0.08 ‰ (1σ) for δ^{18}O.

4 Results

4.1 Site 277 biostratigraphy and stable isotope stratigraphy

Broad age control for DSDP Site 277 is based on the biostratigraphic synthesis of Hollis et al. (1997), who correlated the succession to Southern Hemisphere (SH) radiolarian zones RP6 to RP15. In this study we confirm the location of the base of RP12(SH) (lowest occurrence (LO) of *Lophocyrtis longiventer*) at 371.2–349.2 mbsf, the base of RP14(SH) (LO of *Eucyrtidium spinosum*, 38 Ma) at 264.5–254.5 mbsf, the base of RP15(SH) (LO of *Eucyrtidium antiquum*) at 197.8–186.5 mbsf, and the base of upper Zone RP15(SH) at 143.9–134.5 mbsf (lowest common occurrence (LCO) of *Axoprunum? irregularis*). We revise the base of Zone RP13(SH) to 313.5–312.7 mbsf (LO of *Zealithapium mitra*) (Fig. 2). Further refinement of the age control for Site 277 is possible through application of several additional bioevents, which help to correlate the discontinuous stable isotope record of this site to those from other Southern Ocean sites (Fig. 2). The base of the local New Zealand stage Kaiatan is defined by the highest occurrence (HO) of *Acarinina primitiva* (Morgans, 2009) occurring at 280–273 mbsf based on Jenkins (1975) (39.1 Ma; Raine et al., 2015). We set the base of the Kaiatan at 276.5 mbsf to allow for the correlation between isotope records (Fig. 2). The base of the local Whaingaroan Stage (latest Eocene, 34.6 Ma; Raine et al., 2015) is identified by the HO of *Globigerinatheka index*; this event was identified at 189.6 mbsf by Jenkins (1975), but in the course of preparing foraminifera for stable isotope analysis we have determined that the event occurs slightly higher at 188.58–187.5 mbsf The base of nannofossil zone NP17 (HO of *Chiasmolithus solitus*, 40.4 Ma; Gradstein et al., 2012) is placed at 312.5–301.5 mbsf (Edwards and Perch-Nielsen, 1975). The LCO of *Chiasmolithus*

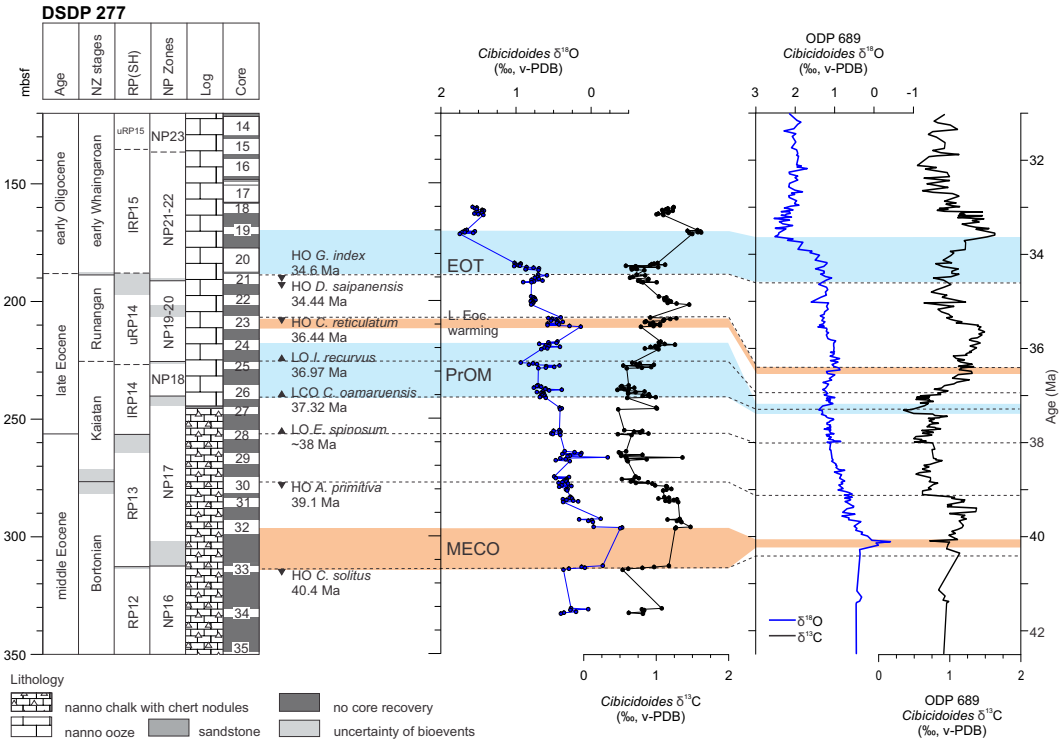

Figure 2. DSDP Site 277 stratigraphy, NZ stages (Raine et al., 2015), Southern Hemisphere radiolarian zones (RP), nannofossil zones (NP), lithology, core recovery, selected bioevents (ages calibrated to the 2012 geological timescale; Gradstein et al., 2012; Raine et al., 2015) and benthic δ^{18}O and δ^{13}C data of DSDP Site 277. The dashed lines correlate with Site 277 based on the ages of the bioevents to Southern Ocean *Cibicidoides* data of ODP Site 689 Hole B (Maud Rise) (Diester-Haass and Zahn, 1996) calibrated to the GTS2012 timescale using the magnetostratigraphy data of Florindo and Roberts (2005) and Spiess (1990). LO: lowest occurrence; LCO: lowest common occurrence; HO: highest occurrence; MECO: Middle Eocene Climatic Optimum; PrOM: Priabonian Oxygen Isotope Maximum; EOT: Eocene–Oligocene transition.

oamaruensis, 37.32 Ma (Gradstein et al., 2012), defines the base of NP18 at 244.5–240.6 mbsf (Edwards and Perch-Nielsen, 1975). The base of NP19-20 is defined by the LO of *Isthmolithus recurvus*, 36.97 Ma (Gradstein et al., 2012), at 226.58–225.5 mbsf (Edwards and Perch-Nielsen, 1975). Within NP19-20, the HO of *Cribrocentrum reticulatum* is found at 206.5–201.1 mbsf (Edwards and Perch-Nielsen, 1975), estimated at 36.44 Ma (Raine et al., 2015). The base of NP21-22 (HO of *Discoaster saipanensis*) is placed at 191.6–190.1 mbsf (Edwards and Perch-Nielsen, 1975) and is dated at 34.44 Ma (Gradstein et al., 2012). As *D. saipanensis* is a warm-water taxon, its disappearance is likely to have occurred earlier at high latitudes. The Eocene–Oligocene boundary is approximated by the HO of *G. index* at DSDP Site 277. More precise location is complicated by incomplete recovery and the highly disturbed nature of cores 277-19R, -20R, and -21R.

Although the recovery gaps in the Site 277 stable isotope record preclude detailed correlation, the broad trends and major events such as the MECO (~ 40 Ma) and PrOM (~ 37.3 Ma) can be identified in the benthic δ^{18}O and δ^{13}C isotope profiles and compared to the middle Eocene–early Oligocene benthic isotope stratigraphy from ODP Site 689 (Maud Rise; Diester-Haass and Zahn, 1996) (Fig. 2). The EOT interval is characterised by a large (~ 1 ‰) positive shift in benthic oxygen and carbon isotopes between cores 277-20R and -19R (183.64–171.28 mbsf) (Shackleton and Kennett, 1975; Keigwin, 1980), which is slightly lower than the full magnitude of the benthic δ^{18}O shift seen at other Southern Ocean sites on the Kerguelen Plateau and Maud Rise (Diester-Haass and Zahn, 1996; Zachos et al., 1996; Bohaty et al., 2012).

4.2 Site 277 oxygen and carbon isotopes

Site 277 δ^{18}O results show a typical surface-to-deep gradient with more negative values in bulk and planktic foraminifers compared to benthic foraminifers (Fig. 3, Supplement Tables 7–10). Foraminiferal δ^{13}C values also display typical gradients, with more positive values in bulk and planktic foraminifers compared to benthic foraminifers (Fig. 3). However, all planktic foraminifera analysed from Site 277 are characterised by a "frosty" preservation state, indicating some diagenetic alteration (Sexton et al., 2006). We have therefore focused our interpretation on benthic foraminifera

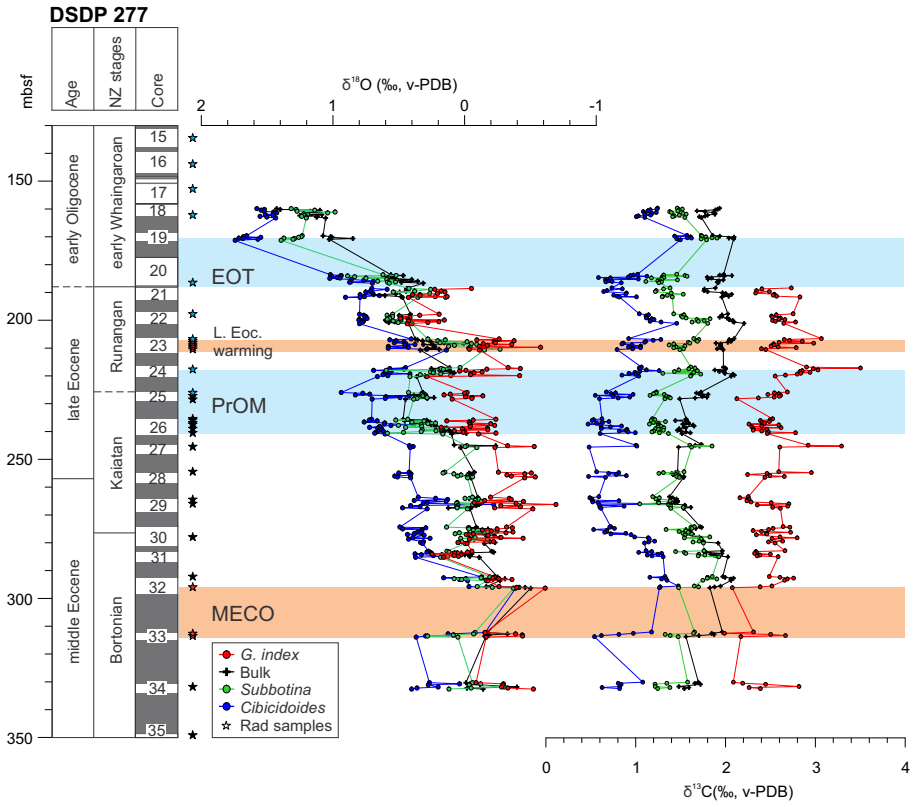

Figure 3. DSDP Site 277 δ^{18}O and δ^{13}C records and location of studied radiolarian samples within the MECO and late Eocene warming interval (red stars) and radiolarian-rich upper Eocene–lower Oligocene interval (blue stars).

because their isotopic signatures are likely less affected by diagenesis.

Several short-lived climatic events are identified in the benthic stable isotope records at Site 277 (Figs. 2 and 3, Supplement Table 7). The body of the MECO was not recovered due to a 16 m sampling gap between the top of Core 277-33R and the base of Core 277-32R, but MECO onset and recovery is well constrained by a 0.5 ‰ negative shift in benthic δ^{18}O values at ~ 313 mbsf (between samples 277-33R-2, 106–108 cm, and -33R-1, 129–130.5 cm) and a ~ 0.4 ‰ positive shift in δ^{18}O values at ~ 296 mbsf (between samples 32R-3, 107–109 cm, and 32R-3, 77–79 cm), indicating that the MECO spans ~ 17 m (Fig. 2). The MECO is more strongly expressed in the benthic δ^{18}O, but this may relate to the poor recovery of the body of the event at this site or diagenetic impacts on planktic δ^{18}O values (Pearson et al., 2001; Sexton et al., 2006). In agreement with other records (Bohaty and Zachos, 2003; Bohaty et al., 2009), a positive δ^{13}C shift is observed in conjunction with the onset of the MECO in the benthic and bulk carbonate records (Fig. 2).

The PrOM event (Scher et al., 2014) is well defined in the δ^{18}O record from DSDP Site 277 but also spans three significant recovery gaps at the base of cores 277-26R, -25R and -24R (~ 244.5 to 225.5 mbsf) (Fig. 3). The ~ 0.4 ‰ positive shift in δ^{18}O that marks the onset of the PrOM spans upper Core 277-26R and lower Core 277-25R (~ 240–230 mbsf) and is followed by an interval of relatively low δ^{18}O values in upper Core 277-25R, prior to reaching maximum values in uppermost Core 277-25R (~ 226 mbsf) (Fig. 2). A gradual decrease in δ^{18}O occurs through Core 277-24R. We define the PrOM at DSDP Site 277 as the interval within these three cores in which benthic δ^{18}O exceeds ~ 0.6 ‰, with the exception of a narrow interval in upper Core 277-25R. These benthic δ^{18}O values are lower than those reported by Scher et al. (2014), but it is likely that peak δ^{18}O values are not captured at Site 277. Consequently, the PrOM is placed between 240.62 and 219.57 mbsf (spanning a ~ 21 m section). The planktic δ^{18}O records show similar trends to the benthic record in the PrOM interval but lack the maximum excursion in uppermost Core 277-25R. At the onset of the PrOM event, short-lived negative δ^{13}C excursions are evident in the benthic, bulk and planktic records. However, a longer-term positive trend for planktic and benthic δ^{13}C values is associated with the benthic δ^{18}O maximum.

Directly above the PrOM event, there is a short-lived ~ 0.4 ‰ decrease in δ^{18}O values in Core 277-23R (210.74 to 207.41 mbsf), evident in benthic and planktic foraminifera as well as bulk carbonate, prior to the increase in δ^{18}O that spans the EOT (Fig. 3). Benthic and planktic δ^{13}C also exhibit a small negative excursion at this level. This interval

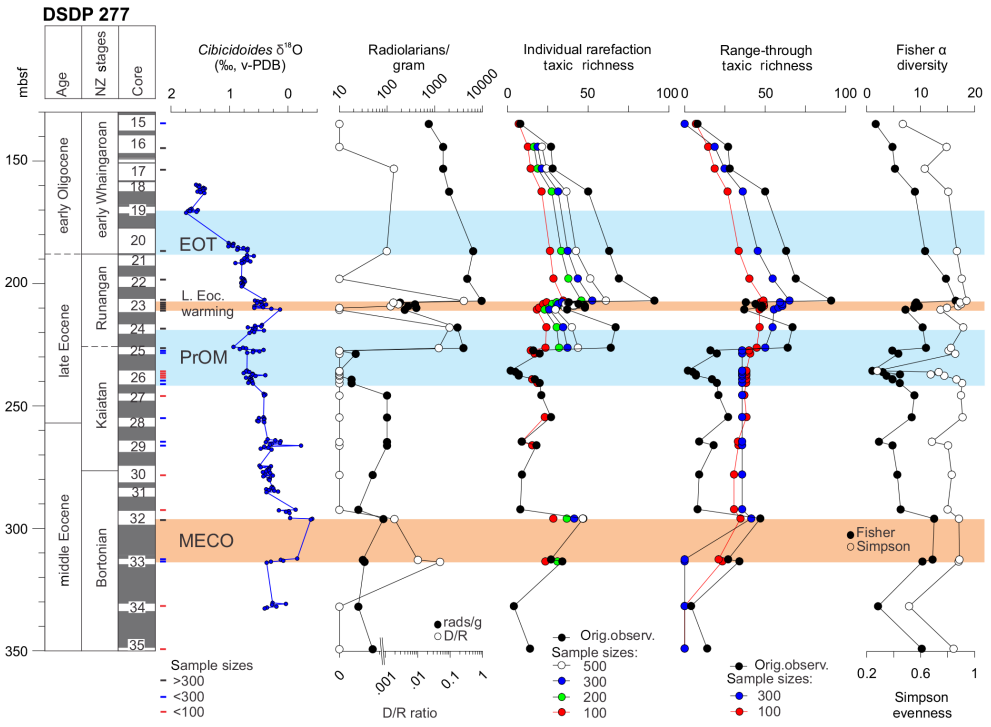

Figure 4. DSDP Site 277 benthic δ^{18}O record, radiolarian abundance and diatom/radiolarian (D/R) ratio, taxic richness (number of taxa) derived from individual rarefaction and range-through analyses for different sample sizes, and Fisher α index and Simpson evenness index for radiolarian assemblages. Red bars indicate sample sizes < 100 specimens, blue bars indicate sample sizes < 300 specimens and black bars indicate samples sizes > 300 specimens.

may be correlated with the late Eocene warming interval reported from ODP sites 689 (Maud Rise), 738, 744, and 748 (Kerguelen Plateau) (Diester-Haass and Zahn, 1996; Bohaty and Zachos, 2003; Villa et al., 2008, 2014).

A large positive shift in δ^{18}O occurs at Site 277 between the base of cores 277-20R and 277-19R, with maximum values in benthic and planktic δ^{18}O and δ^{13}C occurring in Core 277-19R (171.28 to 169.65 mbsf). This can be correlated with the large δ^{18}O shift across the EOT documented at many deep-sea sites, which is characterised by two distinct steps (EOT-1 and Oi-1) in more complete sections (e.g. Coxall et al., 2005; Katz et al., 2008).

We note that the stable isotope record at Site 277 exhibits high-amplitude cyclical variation in the range of 0.5 ‰ for benthic δ^{18}O and slightly more for δ^{13}C (Fig. 3). The presence of at least 10 cycles within the 6 million years between the MECO and the EOT is consistent with orbital-scale forcing. Although the record is too incomplete to establish the frequency of these cycles, their presence in this expanded Palaeogene section bodes well for future drilling at this location.

4.3 Radiolarian assemblages at DSDP Site 277

In total, 16 families, 56 genera and 98 radiolarian species were identified at DSDP Site 277 (Supplement Table 1). Radiolarian abundance is generally low (10–100 specimens g^{-1}) and preservation is moderate throughout the middle Eocene–lower upper Eocene interval (349.2 to 227.2 mbsf) (Fig. 4). In the uppermost Eocene and lower Oligocene (226.1–143.9 mbsf) radiolarians are abundant to very abundant (> 1500 specimens g^{-1}) and well preserved. Diversity increases during the MECO (313.5–296 mbsf) and in the upper Eocene (226.10–186.5 mbsf) and drops in the lower Oligocene (162.2–134.5 mbsf) (Fig. 4). A short-lived drop in radiolarian abundance (< 500 specimens g^{-1}) and diversity is observed at 210.5–207.5 mbsf during the late Eocene warming event. Diversity closely parallels trends in abundance and preservation. Simpson evenness is strongly correlated with diversity but exhibits greater troughs where samples are sparse (Fig. 4). Spumellarians are dominant in most samples ranging between ~ 44 and 96 % (~ 71 % average). The main families are the Actinommidae, Litheliidae, Spongodiscidae, Artostrobiidae, Lychnocaniidae and Lophocyrtiidae (Supplement Table 1).

Three samples from the middle Eocene section of Site 277 (313.5, 312.7, 296 mbsf; cores 277-32R and -33R) that lie within the onset and recovery of the MECO show improved preservation and a peak in diversity and mark the first significant occurrence of diatoms (Fig. 4). *Amphicraspedum murrayanum* and *A. prolixum* gr. have isolated occurrences in this interval, while *A. prolixum* gr.

also has trace occurrences in five samples in the uppermost Eocene to lowermost Oligocene (cores 277-24R to -20R at 217.70, 209, 207.5, 197.82 and 186.50 mbsf). Several species are restricted to the MECO, including *Artobotrys titanothericeraos*, *Sethocyrtis chrysallis*, *Eusyringium fistuligerum* and *Stichopilium* cf. *bicorne*. *Lophocyrtis jacchia hapsis*, which is a high-latitude variant of *L. jacchia jacchia* (Sanfilippo and Caulet, 1998) and endemic to the Southern Ocean, is also common during the MECO and uppermost Eocene (217.7–206.83 mbsf), but is absent from the remaining middle and lower upper Eocene. Furthermore, the LOs of several (albeit rare) species are recorded at this site during the MECO interval (*Axoprunum pierinae*, *Zealithapium mitra*, *Periphaena* spp., *Larcopyle hayesi*, *L. polyacantha*, *Zygocircus buetschli*, *Siphocampe*? *amygdala*, *Eucyrtidium montiparum*, *Lychnocanium amphitrite*, *Clinorhabdus anantomus*, *Lophocyrtis keraspera*, *Lophocyrtis dumitricai*, *Cryptocarpium ornatum* and *Lamprocyclas particollis*) (Supplement Table 1).

A major change in siliceous assemblages occurs within the PrOM interval (∼ 226 mbsf; Core 277-25R), coincident with maximum values in benthic δ^{18}O (Fig. 4). A pronounced increase in radiolarian abundance (from < 50 to ∼ 4000 specimens g^{-1}), preservation and diversity occurs at 226.10 mbsf (Sample 277-25R-1, 60 cm). Diatoms also become abundant at the same level as the increase in radiolarian abundance. The most abundant nassellarian families are the Artostrobiidae (∼ 22 %), Lophocyrtiidae (∼ 6 %) and Lychnocaniidae (∼ 2.5 %). Plagiacanthidae account for ∼ 2 % of the total assemblage. The following taxa have their LO within the PrOM at Site 277: *Lithelius* (?) *foremanae*, *Ceratocyrtis* spp., *Lithomelissa ehrenbergi*, *L. gelasinus*, *L. sphaerocephalis*, *Siphocampe nodosaria*, *Artostrobus annulatus*, *Artostrobus* cf. *pretabulatus*, *Clathrocyclas universa*, *Dictyophimus*? aff. *archipilium*, *Lychnocanium waiareka*, *Aphetocyrtis rossi* and *Theocyrtis tuberosa* (Supplement Table 1).

Five samples were investigated at Site 277 that lie within the late Eocene warming event (210.5–207.5 mbsf). During this event, radiolarian abundance and diversity decrease significantly, as well as diatom abundance (Fig. 4). The radiolarian assemblages of these five samples differ from the other upper Eocene samples. Lychnocaniidae are more abundant (∼ 12 %), whereas Artostrobiidae are absent. Furthermore, Lophocyrtiidae decrease (∼ 4 %) and Plagiacanthidae and *Larcopyle* spp. are very rare (0.5 and 0.9 %, respectively; Supplement Table 1).

Immediately after the warming event, a second pronounced increase in radiolarian abundance (from < 200 to 9600 specimens g^{-1}) and diversity is observed at 206.83 mbsf, together with an increase in diatom abundance (Fig. 4). In the uppermost Eocene–lowermost Oligocene interval (206.83–186.5 mbsf), Plagiacanthidae (∼ 5 %), Artostrobiidae (∼ 7 %) and Lophocyrtiidae (∼ 10 %) increase again, whereas Lychnocaniidae decrease (∼ 2 %; Supplement Table 1). *Theocyrtis tuberosa* has a very rare occurrence from the upper Eocene to lower Oligocene (∼ 226–143.9 mbsf; cores 277-25R to -16R). This species is also known to have had isolated occurrences in the southern Atlantic and southern Indian oceans in the late Eocene (Takemura, 1992; Takemura and Ling, 1997) and is common in latest Eocene to early late Oligocene assemblages from low to middle latitudes of all ocean basins (Sanfilippo et al., 1985).

A significant decline in radiolarian abundance and diversity is observed through the lower Oligocene (186.5 to 134.5 mbsf; cores 277-20R to -15R) (Fig. 4). Radiolarian abundance declines from 6400 to 750 radiolarians g^{-1}. Many nassellarian taxa decline or disappear, especially within the Lophocyrtiidae and Plagiacanthidae. Spumellarians increase from ∼ 73 to ∼ 97 % of the total fauna, with Litheliidae and Actinommidae being the most abundant families (Supplement Table 1).

Rarefaction analysis of Site 277 radiolarian data (Fig. 4) indicates that counts of at least 300 specimens are required to achieve a reliable measure of diversity and taxic richness. However, poor preservation in the middle Eocene and lower upper Eocene intervals (∼ 350 to ∼ 227 mbsf) has resulted in poor recovery of radiolarians, with 9 samples containing < 300 specimens and 9 samples of < 100 specimens. Because these samples span an interval in which significant changes in diversity and assemblage composition occur, we include metrics for all samples in Fig. 4 (samples of < 100 specimens, < 300 specimens and > 300 specimens are highlighted) and metrics for samples with > 100 specimens in Figs. 6 and 7. To investigate whether the diversity drop between ∼ 292 and ∼ 227 mbsf is a preservational artefact or a real feature of the assemblage, we also determined range-through taxic richness (Fig. 4). We have chosen sample sizes of 100 and 300 (both with a subsampling of 1000), which show a similar pattern to the original observation. The decrease in range-through taxic richness at the top and bottom of the record is due to edge effects. According to this analysis, range-through taxic richness is higher than observed in cores 277-32 to -26 (292.2–235.5 mbsf). Chert nodules are present down-core from ∼ 246 mbsf, so the scarcity of taxa in the interval between ∼ 350 and 246 mbsf is likely to be an artefact of diagenesis. However, the increase in taxic richness in the MECO appears to be supported by this analysis, at least for the uppermost sample. The analysis also indicates that there is a distinct increase in diversity related to the PrOM event around ∼ 226 mbsf, although it is more muted than the raw data suggest. It is notable that the decrease in diversity evident in the raw data during the late Eocene warming event is not shown in the range-through data. In fact, there may be a further increase in taxic richness within this interval. We conclude that range-through taxic richness is a helpful tool for determining whether diversity changes are due to diagenesis or environmental variation, especially when coupled with consideration of the lithologic changes (e.g. chertification).

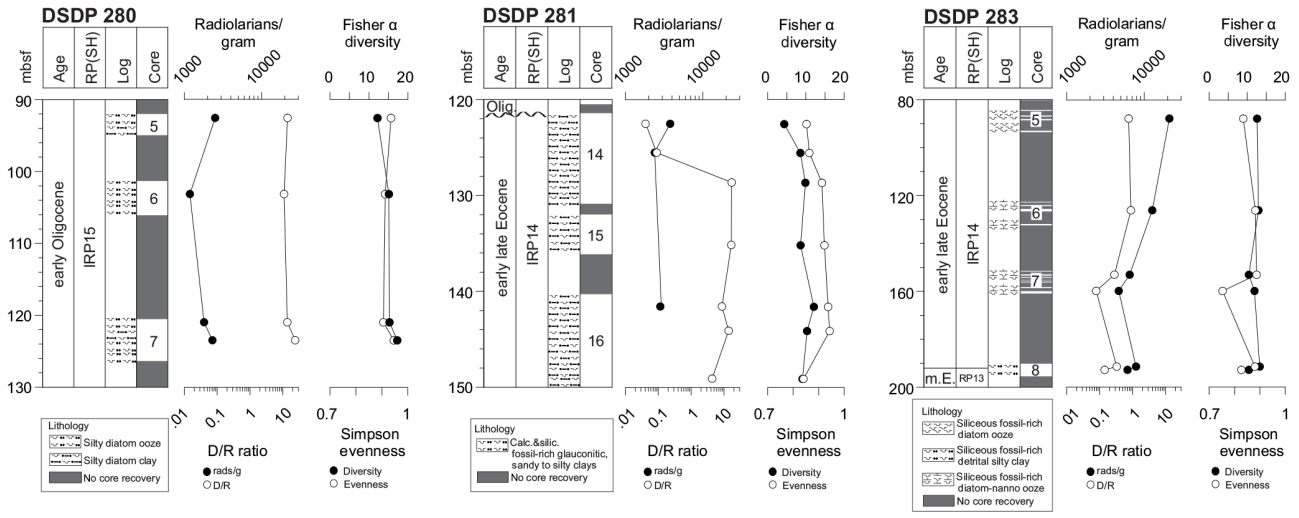

Figure 5. Stratigraphy, Southern Hemisphere radiolarian zones (RP), lithology and core recovery at DSDP sites 280, 281 and 283. Variation in radiolarian abundance, diatom / radiolarian (D/R) ratio, Fisher α index and Simpson evenness for radiolarian assemblages at all sites.

4.4 Radiolarian assemblages at other southwest Pacific sites

To establish the significance and nature of radiolarian faunal turnover associated with the PrOM event regionally, we investigated the upper Eocene–lower Oligocene intervals of DSDP sites 280, 281 and 283 and ODP Site 1172.

4.4.1 DSDP Site 280

Four samples were investigated at DSDP Site 280 from cores 280-7R, -6R and -5R (123.4 to 92.54 mbsf). In previous work, the Eocene–Oligocene boundary in Hole 280 was placed at the base of Core 280-6R (110.5 mbsf) (Crouch and Hollis, 1996). However, due to the presence of *Eucyrtidium antiquum* (Caulet, 1991) and *Larcopyle frakesi* (Chen, 1975), both of which have LOs in the lower Oligocene, we place the studied interval (123.4–92.54 mbsf) in lower Oligocene Zone RP15(SH) (Fig. 5, Supplement Table 3). This is in agreement with O'Connor (2000), who found upper Eocene assemblages were restricted to cores 280-10R to -8R (205.5 to 139 mbsf). The absence of the zonal marker *Axoprunum? irregularis* indicates correlation with lower RP15(SH) *Eucyrtidium spinosum*, which according to Funakawa and Nishi (2005) has its HO in the lower Oligocene, is absent in the Site 280 study interval. However, the HO of this species is recorded within the upper Eocene interval at Site 277, suggesting a diachronous HO between the southwest Pacific and the South Atlantic.

In total, 15 families, 35 genera and 50 radiolarian species were identified at Site 280. Radiolarians are abundant (1000–2500 specimens g^{-1}) and well preserved in all samples. Diatoms are also very abundant (D/R ratio $\sim$10) (Fig. 5). Diversity and evenness are stable and high in all samples. Spumellarians are slightly more abundant than nassellarians (52–66 % of the assemblage). The most abundant families are Litheliidae (20–37 %), Plagiacanthidae (14–22 %), Actinommidae (4–12 %), Spongodiscidae (5–9 %), Eucyrtidiidae (4–8 %) and Lophocyrtiidae (3–8 %) (Supplement Table 3). Compared to DSDP Site 277, this site has higher diatom abundance and better overall preservation, which may explain the higher diversity. More species of the genera *Lithomelissa* (7) and *Larcopyle* (5) are present, as well as a higher abundance of Lophocyrtiidae. Lychnocaniids are very rare at this site (< 1 %) and the genus *Lychnocanium* is absent (Supplement Table 3).

4.4.2 DSDP Site 281

Seven samples were investigated from DSDP Site 281 in the interval between 149 and 122.5 mbsf (cores 281-16R to -14R) (Fig. 5). Results from three of these samples were previously reported in Crouch and Hollis (1996) but have been re-examined for this study. Due to the presence of *Eucyrtidium spinosum* and *Eucyrtidium nishimurae*, the latter with a HO in the late Eocene at $\sim$36.9–36.7 Ma (Funakawa and Nishi, 2005), we correlate the Site 281 study interval with lower Zone RP14(SH) ($\sim$ Kaiatan local stage). A hiatus spanning the uppermost Eocene and Oligocene is inferred from the presence of abundant glauconite in the upper part of Core 281-14R as well as from common *Cyrtocapsella tetrapera* in Core 281-13R, which indicates a Miocene age (Crouch and Hollis, 1996).

In total, 14 families, 34 genera and 46 species were identified at Site 281. Radiolarians are abundant (2000–4000 specimens g^{-1}) and well preserved. Diversity is lower than at Site 280, but evenness is still high and similar to the other sites (Fig. 5). The D/R ratio is also high and comparable to Site 280, except in the upper two samples in Core

281-14R (125.5–122.5 mbsf). The radiolarian assemblages are dominated by spumellarians (55–93 %), with Litheliidae (17–42 %), Spongodiscidae (12–30 %) and Actinommidae (10–20 %) the most abundant families. The most common nassellarians belong to the Plagiacanthidae (1–15 %), Lophocyrtiidae (3–7 %) and Eucyrtidiidae (1–7 %) (Supplement Table 4). Although sites 280 and 281 were relatively close to each other (Fig. 1), the radiolarian assemblages are distinctly different, indicating different oceanographic conditions. Crouch and Hollis (1996) concluded that Site 281 was shallower and closer to terrigenous influx than Site 280. The depositional environment of Site 280 is interpreted as more oceanic. The greater abundance of Spongodiscidae at Site 281 supports a shallower oceanic setting for this locality (Casey, 1993). Compared to the early upper Eocene assemblage of Site 277, where radiolarian abundance and diversity is very low, with several samples containing less than ∼ 100 specimens, Site 281 contains more Spongidiscidae (∼ 20 %), Plagiacanthiidae (∼ 7 %) and Litheliidae (∼ 20 %), whereas the genus *Lychnocanium* is absent at Site 281.

4.4.3 DSDP Site 283

Six samples were examined from Site 283 between 192.25 and 87.75 mbsf (cores 283-8R to -5R) (Fig. 5). The lowermost sample at 192.25 mbsf is correlated with RP13(SH) due to the absence of *Eucyrtidium spinosum*. The uppermost five samples are of early late Eocene age based on the presence of *E. spinosum* and nannofossil age control (Edwards and Perch-Nielsen, 1975). The age of the Site 281 and 283 successions are poorly defined and the PrOM event cannot be located at these sites. Both sites contain *Eucyrtidium nishimurae*: at Site 283 it is found in all samples, and at Site 281 its HO is in 125.5–122.5 mbsf. According to Funakawa and Nishi (2005) its HO is in C17n1n (∼ 36.7 Ma; Gradstein et al., 2012). *E. nishimurae* is absent at Site 277. The deposition of siliceous ooze in the upper middle to upper Eocene and the absence (or very rare) occurrence of foraminifera suggests a deep oceanic setting close or below the calcite compensation depth (CCD) for Site 283.

A total of 16 families, 50 genera and 81 radiolarian species were recorded at Site 283. Radiolarians are very abundant (4700–21 150 radiolarians g^{-1}) – with the highest abundance in cores 283-6R and -5R – well preserved, and diverse (59–77 taxa per sample, Fisher α index of 10–13, evenness of 0.75–0.89). Diatoms are present in low abundance with D/R ratios < 1 (Fig. 5). Spumellarians account for 59–87 % of the assemblage, with the Litheliidae (23–38 %), Actinommidae (5–19 %) and Spongodiscidae (2–8 %) the most abundant families. The Trissocyclidae (2–11 %), Eucyrtidiidae (2–11 %), Lophocyrtiidae (3–8 %) and Plagiacanthidae (2–8 %) are the most common nassellarian families (Supplement Table 5). *Theocyrtis tuberosa* is very abundant in the uppermost sample. The acme of this taxon might be correlated with its rare occurrence at Site 277 in the upper Eocene. Several taxa appear earlier at Site 283 than at Site 277. These include the following taxa that occur in the upper middle Eocene (e.g. *Axoprunum bispiculum*, *Amphicentria* sp. 1 sensu Suzuki, *Ceratocyrtis* spp., *Lithomelissa ehrenbergi*, *L.* cf. *haeckeli*, *L. sphaerocephalis*, *L. tricornis*, *Pseudodictyophimus gracilipes* gr., *Tripodiscinus clavipes*, *Siphocampe nodosaria*, *Spirocyrtis joides*, *Aspis* sp. A sensu Hollis, *Clathrocyclas universa*, *Eurystomoskevos petrushevskaae*, *Lychnocanium waiareka*, *Aphetocyrtis gnomabax*) or lower upper Eocene (*Spirocyrtis greeni*, *Eurystomoskevos cauleti*, *Lophocyrtis jacchia hapsis*, *Lamprocyclas particollis*) at Site 283.

4.4.4 ODP Site 1172

Forty-one samples were analysed from ODP Site 1172 spanning the middle Eocene–lower Oligocene interval, including four samples from Core 1172D-2R (356.875–355.675 mbsf) and 37 from cores 1172A-48X to -39X (445.01–354.625 mbsf). The faunal assemblages of ODP Site 1172 were described by Suzuki et al. (2009), who did not correlate them to RP zones. Many taxa used to define Southern Hemisphere RP zones at Site 277 are absent at Site 1172 or have diachronous ranges. *Eucyrtidium spinosum*, the marker for Zone RP14(SH), has its LO at 373.75–371.21 mbsf, but *Lithomelissa tricornis* and *Pseudodictyophimus gracilipes* are absent. *Eucyrtidium antiquum* has a single LO at 365.21 mbsf, but is absent in the early Oligocene. *E. nishimurae* is present within the middle and upper Eocene. *Axoprunum irregularis* is very abundant in the lower Oligocene interval at this site (356.875–354.625 mbsf), which we correlate to the upper RP15(SH) zone.

Spumellarians dominate the Site 1172 assemblages throughout the middle Eocene to lower Oligocene (∼ 82 %). The Litheliidae are the most abundant family, comprising about 20 % on average in the middle Eocene, 35 % in the upper Eocene, and 25 % in the lower Oligocene. Plagiacanthidae (0.5–2.5 %), Eucyrtidiidae (0.5–3 %), Lophocyrtiidae (1.5–8 %) and Lychnocaniidae (0.5–2.7 %) account for most of the nassellarians. Fisher α diversity and Simpson evenness are very high throughout the succession, ranging between ∼ 10 and 20 and between 0.82 and 0.96, respectively. Similar to Site 277, diversity and evenness decrease in the lower Oligocene (Supplement Table 6).

Eocene sediments at Site 1172 consist of silty claystone with abundant diatoms. This sequence is overlain by a transitional unit in the uppermost Eocene consisting of glauconitic siltstones, which indicate increased bottom-water current activity in the uppermost Eocene (Kennett and Exon, 2004; Stickley et al., 2004). There is a sharp transition in the lowermost Oligocene to a pelagic carbonate sequence consisting of nannofossil chalk (Exon et al., 2004). Diatoms are more abundant and of inner neritic nature in the middle Eocene until ∼ 408 mbsf (∼ 39 Ma), where they become more oceanic and may indicate a change to a more outer neritic regime.

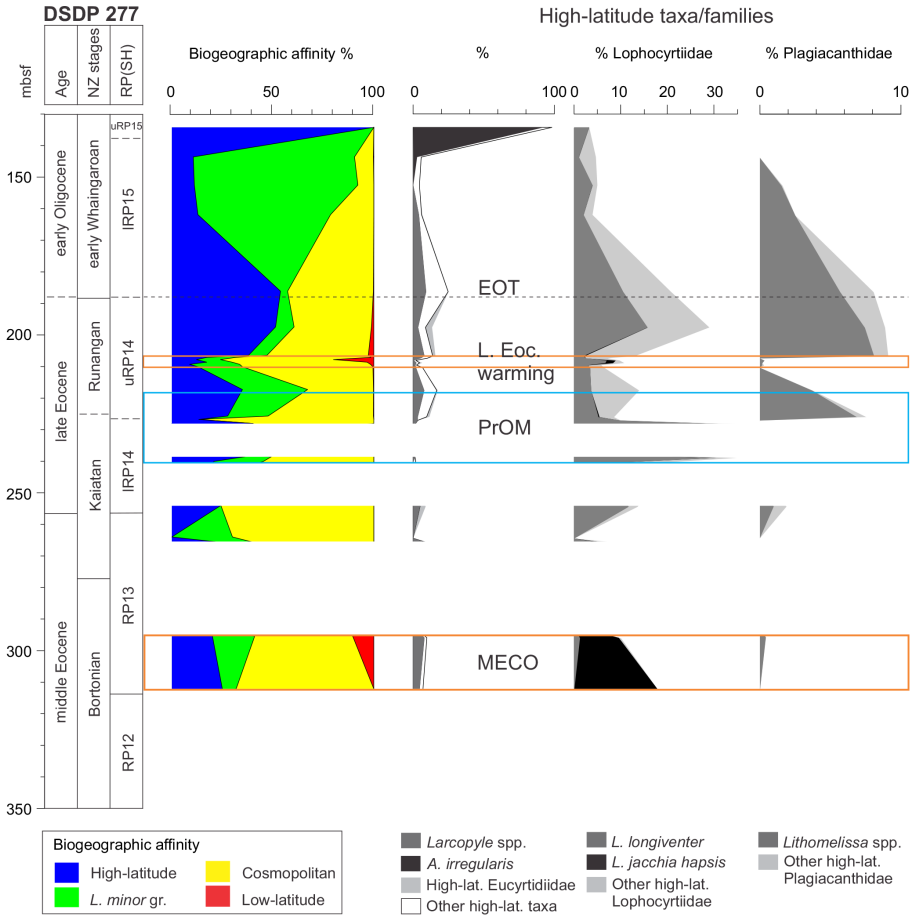

Figure 6. Biogeographic affinities of radiolarian assemblages at DSDP Site 277 and the abundance of high-latitude taxa/families. MECO: Middle Eocene Climatic Optimum; PrOM: Priabonian Oxygen Isotope Maximum; EOT: Eocene–Oligocene transition.

Above ∼376 mbsf (∼38 Ma) the diatom assemblage indicates an inner to outer neritic regime (Röhl et al., 2004).

4.5 Trends in biogeographic affinities

The radiolarian assemblages at our five sites include 92 species or species groups that can be assigned to one of three biogeographic categories: high latitude (50 taxa), cosmopolitan (38 taxa), and low latitude (4 taxa) (Table 1, Supplement Table 12). Biogeographic affinities remain poorly known for the remaining 39 taxa encountered at DSDP sites 277, 280, 281 and 283, and for ∼100 taxa at Site 1172 reported by Suzuki et al. (2009). Within the high-latitude group, six taxa are bipolar (*Artostrobus annulatus*, *Axoprunum bispiculum*, *Ceratocyrtis* spp., *Cycladophora cosma cosma*, *Pseudodictyophimus gracilipes* gr. and *Spongopyle osculosa*), whereas 45 taxa are inferred to be endemic to the Southern Ocean. Almost all species in the Litheliidae, Lophocyrtiidae and Plagiacanthidae are high latitude. The biogeographic affinity of *Lithelius minor* gr. is considered to be cosmopolitan, but because this group is very abundant in some assemblages, we separate it out in Figs. 6 and 7. For Site 277, we also differentiate key high-latitude taxa within the three families noted above, namely *Larcopyle* spp., *Lophocyrtis longiventer* and *Lithomelissa* spp., and the actinommid *Axoprunum irregularis* (Fig. 6).

At Site 277, taxa with high-latitude affinities are present from the base of the study section in the middle Eocene (Fig. 6). The MECO is characterised by the presence of high-latitude taxa of ∼23 % (*Larcopyle* spp., *Lophocyrtis jacchia hapsis*, *L. longiventer*), but also the appearance of low-latitude species *Amphicraspedum murrayanum* and *A. prolixum* gr. (up to ∼10 %). *Lophocyrtis jacchia hapsis* is considered to be a high-latitude variant of *L. jacchia jacchia* and has a short stratigraphic range in the middle to late Eocene in the Southern Ocean (Sanfilippo and Caulet, 1998). In our study this taxon has a common appearance only during the MECO and in the upper Eocene (Fig. 6). In the middle of the PrOM event (∼225 mbsf), diversity and high-latitude taxa increase (average of 28 %) in conjunction with the appearance of *Lithomelissa* spp. and other high-latitude Lophocyrtiidae.

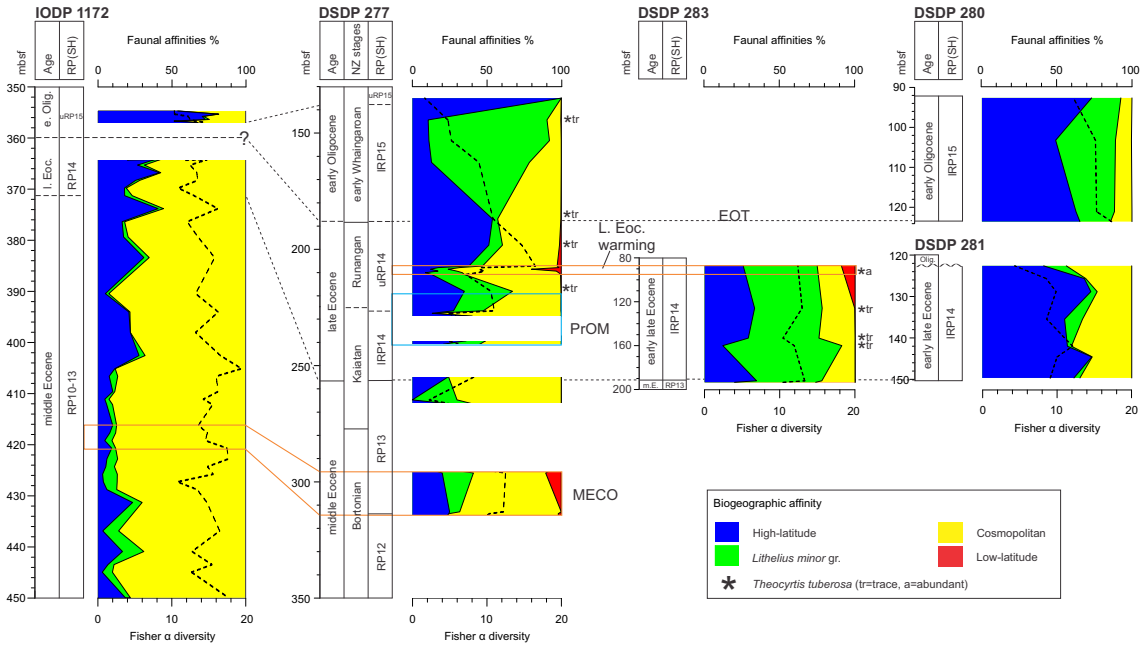

Figure 7. Variation in faunal affinities for radiolarian assemblages and Fisher α diversity at all sites. Dashed black lines indicate correlation between sites. The location of the MECO at Site 1172 is taken from Bijl et al. (2010).

During the late Eocene warming event, high-latitude taxa decrease to ∼ 13 % at Site 277 and only rare occurrences of *Lithomelissa* spp. and high-latitude *Lophocyrtis* spp. are noted (Fig. 6, Table 2). Late Eocene warming, however, coincides with the abundant occurrence of the low-latitude taxon *Thyrsocyrtis pinguisicoides* (up to 20 %) and the trace occurrence of *A. prolixum*. Cosmopolitan taxa are dominated by *Lychnocanium* spp., but general diversity also decreases within the warming event (Supplement Table 1). After this event, high-latitude taxa increase to up to ∼ 50 % in the uppermost Eocene and lowermost Oligocene with the reappearance of all high-latitude taxa and an overall diversification (Fig. 6, Table 2). During the lower Oligocene, diversity declines and especially the Plagiacanthidae and Lophocyrtiidae decrease in abundance. *Lithelius minor* gr. is dominant until ∼ 144 mbsf Above 144 mbsf, *Lithelius minor* gr. decreases in abundance and high-latitude actinommids *Axoprunum bispiculum* and *A. irregularis* make up ∼ 97 % of the high-latitude assemblage (Fig. 6, Supplement Table 1).

At Site 1172, high-latitude taxa are present in the middle and upper Eocene, although varying between ∼ 3 and 40 % of the assemblage for which biogeographic affinities have been established (Fig. 7). The MECO interval at Site 1172 (Core 1172D-45X; Bijl et al., 2010) corresponds to a minimum in high-latitude taxa, which is part of a longer minimum in high-latitude taxa from 430 to 410 mbsf The most profound increase in high-latitude taxa at Site 1172 occurs in the lower Oligocene (∼ 50–80 %) with an increase in abundance of *A. irregularis* to dominant levels, similar to Site 277. None of the low-latitude taxa found at the other sites are present at Site 1172.

At Site 283, high-latitude taxa are present from the middle Eocene and range between ∼ 12 and 35 %. *Lithelius minor* gr. is very abundant and varies between ∼ 20 and 40 % in all samples (Fig. 7). We tentatively correlate the relatively high abundance in the low-latitude species *Theocyrtis tuberosa* (∼ 9 %) in the upper part of the studied section (87.75 mbsf) to the late Eocene warming event at Site 277. Sites 280 and 281 both have a higher proportion of high-latitude taxa in the lower upper Eocene to lower Oligocene than all other sites. High-latitude taxa range between ∼ 40 and 73 % in the lower upper Eocene at Site 281 and between ∼ 50 and 73 % in the lower Oligocene at Site 280 (Fig. 7). Several taxa that are present in the lower Oligocene at Site 280 are absent at Site 277, including *Lithomelissa challengerae*, *Larcopyle frakesi*, *Lithomelissa sakaii*, and *Antarctissa* spp. The abundance of *Lithelius minor* gr. is also high at sites 280 and 281, ranging between ∼ 20 and 40 %.

5 Discussion

5.1 Comparison with geochemical temperature proxies

The radiolarian assemblages documented at sites 277 and 1172 within the MECO interval lack typical tropical taxa such as *Thyrsocyrtis* spp. or *Podocyrtis* spp. (e.g. Kamikuri et al., 2013). Taxa with low-latitude affinities, such as *Amphicraspedum murrayanum* and *A. prolixum* gr., account for only 5 % of the total assemblage at Site 277 and are absent at

Table 1. Summary of species for which biogeographic affinities have been established and their presence (x) at sites 277, 280, 281, 283, and 1172. H: high latitude (> 45° N/S); L: low latitude (< 25° N/S); and C: cosmopolitan. Location of photographic images on plates for selected species.

Taxa	Biogeogr. affinity	Site 277	Site 280	Site 281	Site 283	ODP1172	Plate
Amphicentria sp. 1 sensu Suzuki	H	x		x	x	x	Pl. 2, Fig. 1
Amphicraspedum murrayanum Haeckel	L	x					Pl. 1, Fig. 14
Amphicraspedum prolixum Sanfilippo and Riedel gr.	L	x	x				Pl. 1, Figs. 15–17
Amphisphaera coronata (Ehrenberg) gr.	C	x			x	x	Pl. 1, Fig. 2
Amphisphaera spinulosa (Ehrenberg)	C	x			x		Pl. 1, Fig. 5
Amphymenium splendiarmatum Clark and Campbell	C	x	x	x	x		Pl. 1, Figs. 18, 19
Antarctissa cylindrica Petrushevskaya	H		x				
Antarctissa robusta Petrushevskaya	H		x				
Aphetocyrtis bianulus (O'Connor)	H	x			x	x	Pl. 5, Fig. 1
Aphetocyrtis gnomabax Sanfilippo and Caulet	H	x	x	x	x		Pl. 5, Figs. 2–7
Aphetocyrtis rossi Sanfilippo and Caulet	H	x	x		x		Pl. 5, Figs. 8–11
Artobotrys auriculaleporis (Clark and Campbell)	C	x				x	
Artostrobus annulatus (Bailey)	H	x			x		
Artostrobus cf. *pretabulatus* Petrushevskaya	H	x					Pl. 3, Fig. 13
Aspis sp. A sensu Hollis	H	x	x		x		Pl. 3, Figs. 14–16
Axoprunum bispiculum (Popofsky)	H	x			x		
Axoprunum pierinae (Clark and Campbell) gr.	C	x	x	x	x	x	Pl. 1, Figs. 10, 11
Axoprunum? *irregularis* Takemura	H	x				x	Pl. 1, Fig. 12
Ceratocyrtis spp.	H	x	x		x	x	Pl. 2, Figs. 3–5
Cinclopyramis circumtexta (Haeckel)	C	x	x	x	x	x	
Clathrocyclas universa Clark and Campbell	C	x		x	x	x	
Clinorhabdus anantomus Sanfilippo and Caulet	H	x		x	x		Pl. 5, Figs. 12, 13
Clinorhabdus robusta (Abelmann)	H					x	
Cornutella profunda Ehrenberg	C	x	x	x	x	x	
Cryptocarpium bussonii (Carnevale) gr.	C	x	x	x	x	x	Pl. 5, Figs. 25a, b, 26a, b
Cryptocarpium ornatum (Ehrenberg)	C	x			x		
Cycladophora cosma cosma Lombari and Lazarus	H		x				Pl. 3, Fig. 17
Cycladophora humerus (Petrushevskaya)	H		x	x	x		Pl. 3, Fig. 18
Cycladophora spp.	H	x		x	x		
Cyrtolagena laguncula Haeckel	C	x			x		
Dictyophimus pocillum Ehrenberg	C	x					
Dictyophimus? aff. *archipilium* Petrushevskaya	H	x		x	x		Pl. 4, Fig. 3a, b–8
Dictyophimus? *archipilium* Petrushevskaya	H	x	x		x		Pl. 4, Figs. 1a, b, 2
Eucyrtidium antiquum Caulet	H	x	x			x	Pl. 3, Fig. 19
Eucyrtidium mariae Caulet	H	x					
Eucyrtidium nishimurae Takemura and Ling	H			x	x	x	Pl. 3, Fig. 20a, b
Eucyrtidium spinosum Takemura	H	x		x	x	x	Pl. 3, Fig. 21
Eucyrtidium montiparum Ehrenberg	C	x			x		Pl. 3, Fig. 22
Eurystomoskevos cauleti O'Connor	H	x	x	x	x		Pl. 3, Fig. 23a, b
Eurystomoskevos petrushevskaae Caulet	H	x	x	x	x	x	Pl. 3, Fig. 24
Eusyringium fistuligerum (Ehrenberg)	C	x				x	Pl. 3, Fig. 25
Eusyringium lagena (Ehrenberg)	C				x		
Glycobotrys nasuta (Ehrenberg) gr.	C	x	x	x	x	x	Pl. 3, Figs. 5–7
Lamprocyclas particollis O'Connor	H	x	x	x	x		Pl. 5, Fig. 27
Larcopyle cf. *pylomaticus* (Riedel)	H		x	x			Pl. 1, Fig. 25a, b
Larcopyle frakesi (Chen)	H		x				Pl. 1, Fig. 20
Larcopyle hayesi (Chen)	H	x	x	x	x		Pl. 1, Fig. 21
Larcopyle labyrinthusa Lazarus	H		x				Pl. 1, Fig. 22
Larcopyle polyacantha (Campbell and Clark) gr.	H	x	x	x	x		Pl. 1, Figs. 23, 24
Larcopyle spp.	H	x	x	x			
Lithelius minor Jörgensen gr.	C	x	x	x	x	x	Pl. 1, Figs. 26–28
Lithomelissa challengerae Chen	H		x				Pl. 2, Figs. 6–8
Lithomelissa ehrenbergi Bütschli	H	x	x	x	x	x	Pl. 2, Figs. 10, 11
Lithomelissa gelasinus O'Connor	H	x	x	x	x		Pl. 2, Figs. 12, 13
Lithomelissa robusta Chen	H		x		x		Pl. 2, Fig. 16
Lithomelissa sphaerocephalis Chen	H	x	x	x	x		Pl. 2, Fig. 17
Lithomelissa spp.	H	x	x	x	x		
Lithomelissa tricornis	H	x	x	x	x		Pl. 2, Fig. 18
Lithomelissa? *sakaii* O'Connor	H		x				Pl. 2, Fig. 19
Lophocyrtis (Apoplanius) *aspera* (Ehrenberg)	H	x		x	x		Pl. 5, Figs. 14a, b–16
Lophocyrtis (Apoplanius) *keraspera* Sanfilippo and Caulet	H	x			x	x	Pl. 5, Figs. 17–19
Lophocyrtis (Lophocyrtis) *jacchia hapsis* Sanfilippo and Caulet	H	x			x		Pl. 5, Figs. 20–22
Lophocyrtis (*Paralampterium*) *dumitricai* Sanfilippo	C	x				x	

Table 1. Continued.

Taxa	Biogeogr. affinity	Site 277	Site 280	Site 281	Site 283	ODP1172	Plate
Lophocyrtis (*Paralampterium*) *longiventer* (Chen)	H	x	x	x	x	x	Pl. 5, Figs. 23, 24
Lophocyrtis spp.	H				x		
Lophophaena capito Ehrenberg	C	x		x	x		
Lychnocanium amphitrite (Foreman)	C	x			x	x	Pl. 4, Figs. 11a, b, c, 12
Lychnocanium babylonis (Clark and Campbell)	C	x			x		Pl. 4, Figs. 13a, b, 14
Lychnocanium bellum Clark and Campbell	C	x			x	x	Pl. 4, Figs. 15, 16
Periphaena decora Ehrenberg	C	x	x	x	x	x	
Periphaena heliastericus (Clark and Campbell)	C	x	x	x	x	x	
Plectodiscus circularis (Clark and Campbell)	C	x	x	x	x	x	
Pseudodictyophimus galeatus Caulet	H		x				Pl. 2, Fig. 20
Pseudodictyophimus gracilipes (Bailey) gr.	H	x	x	x	x		Pl. 2, Figs. 21–23
Pseudodictyophimus spp.	H		x				Pl. 2, Figs. 24–27
Sethocyrtis chrysallis Sanfilippo and Blome	C	x					Pl. 3, Fig. 26a, b
Siphocampe nodosaria (Haeckel)	C	x		x	x	x	
Siphocampe quadrata (Petrushevskaya and Kozlova)	C	x		x	x	x	
Siphocampe? *amygdala* (Shilov)	C	x			x		Pl. 3, Figs. 11, 12
Sphaeropyle tetrapila (Hays)	H	x					Pl. 1, Fig. 29
Spirocyrtis joides (Petrushevskaya)	C	x	x	x	x		
Spongodiscus cruciferus (Clark and Campbell)	C	x		x		x	
Spongodiscus festivus (Clark and Campbell)	C	x				x	
Spongopyle osculosa Dreyer	H	x	x	x	x	x	Pl. 1, Fig. 13
Spongurus bilobatus Clark and Campbell	C	x		x	x	x	
Stylosphaera minor Clark and Campbell gr.	C	x	x		x	x	Pl. 1, Fig. 7
Theocampe amphora (Haeckel)	C	x					
Theocampe urceolus (Haeckel)	C	x	x	x	x		
Theocyrtis tuberosa Riedel	L	x			x		Pl. 5, Fig. 30
Thyrsocyrtis pinguisicoides O'Connor	L	x			x		Pl. 3, Fig. 27
Tripodiscinus clavipes (Clark and Campbell)	C	x		x	x		
Zealithapium mitra (Ehrenberg)	C	x			x		Pl. 1, Fig. 8

Table 2. Average of total % of high-latitude species, groups, genera and high-latitude members of families for five time slices: Middle Eocene Climatic Optimum (MECO, ∼ 40 Ma), early late Eocene/PrOM (∼ 38–37 Ma), late Eocene warming event (∼ 36 Ma), latest Eocene–earliest Oligocene (∼ 35–32 Ma) and early Oligocene (∼ 30 Ma).

	Site 277					Site 280	Site 281	Site 283		Site 1172		
	40 Ma	38–37 Ma	36 Ma	35–32 Ma	30 Ma	earliest Olig.	38–37 Ma	38–37 Ma	36 Ma	40 Ma	late Eoc.	30 Ma
% high-latitude species	23.2	28.9	13.7	39.0	100.0	62.6	61.2	28.0	25.6	7.8	26.8	66.1
Larcopyle spp. %	6.9	2.9	2.5	6.2	–	18.4	26.5	3.0	1.8	–	–	7.0
Lithomelissa spp. %	0.1	1.8	0.1	5.9	–	16.4	11.8	4.1	4.8	0.4	0.7	0.8
High-lat. Lophocyrtiidae %	14.9	20.8	8.0	16.7	3.3	10.4	14.2	8.5	6.9	4.1	19.3	5.7
High-lat. Eucyrtidiidae %	–	0.4	0.5	1.8		8.8	6.3	7.4	9.1	3.3	5.3	–
Other high-lat. Plagiacanthidae %	–	0.2	–	1.4		6.5	1.4	1.8	1.5	–	–	0.2
Other high-lat. species %	1.3	2.8	2.7	7.0	96.7	2.0	1.1	3.1	1.5	0.1	1.6	52.5
% cosmopolitan species	72.6	71.1	80.9	59.9	–	37.3	38.8	71.8	65.2	92.2	73.2	33.9
% low-latitude species	4.2	0.1	5.4	1.0	–	0.1	–	0.1	9.2	–	–	–

Site 1172. The persistence of high-latitude taxa and the variety of cosmopolitan species at both sites suggests a warm temperate climate (15–20 °C; Nelson and Cooke, 2001), in contrast to geochemical proxies suggesting a tropical climate (> 25 °C) for the MECO at Site 1172 (Bijl et al., 2010) and ∼ 27 °C for the latest Eocene at Site 277 (Liu et al., 2009). The sea surface temperature estimates were derived from organic proxies (TEX_{86} and $U^{K'}_{37}$) and may be biased towards summer temperatures (Liu et al., 2009; Hollis et al., 2012). Although the interval of peak warmth may not be preserved in the MECO at Site 277, the relatively low abundance of tropical radiolarian taxa within the Palaeocene–Eocene Thermal Maximum and early Eocene climatic optimum in the southwest Pacific has also been previously noted by Hollis (2006; Hollis et al., 2014).

5.2 Nature of the Antarctic assemblage

High-latitude taxa existed from at least the middle Eocene at sites 277, 283 and 1172. Many taxa that are present from the earliest late Eocene (∼ 38 Ma) at sites 281 and 283 appear later at Site 277, during the PrOM event (∼ 37 Ma), coinciding with an increase in radiolarian abundance, diversity and preservation. A comparison of all high-latitude groups

is shown in Table 2. We assigned all *Lithomelissa* spp. and *Larcopyle* spp. to the high-latitude group as they are more abundant at higher-latitude sites. Although we assigned a cosmopolitan affinity to *Lithelius minor* gr., the palaeoecology of this group is not yet fully understood, as it tends to be most abundant at high-latitude sites. The sudden appearance of *Lithomelissa* spp. and other high-latitude taxa and diatoms at Site 277 indicates the expansion of high-latitude water masses across the southern Campbell Plateau in two phases: first during the PrOM event and again after the late Eocene warming event when a second diversification and influx of high-latitude taxa is observed.

5.3 High-latitude cooling and eutrophication during the PrOM event

5.3.1 Diagenesis

One possible explanation for the pronounced increase in radiolarian abundance and diversity in the upper Eocene at Site 277 is that these trends are an artefact of biogenic opal diagenesis. Chert nodules are recorded throughout the upper Palaeocene–middle Eocene section of the cored sequence at Site 277, with a transition between chert-bearing nannofossil chalk and overlying nannofossil ooze at 246 mbsf (lower upper Eocene) (Kennett et al., 1975). The presence of chert combined with the generally poorer preservation of radiolarians in the lower Palaeogene interval indicates some degree of diagenesis, which is also reflected in the range-through taxic richness analysis. However, the first major radiolarian turnover event occurs ∼ 20 m above the lithological transition from chert-bearing nannofossil chalk to nannofossil oozes, which implies that the event represents a real increase in radiolarian and diatom abundance and not an artefact of diagenesis. No lithological changes are present at that level, which could explain the observed diversity decrease during the late Eocene warming event and the increase in diversity thereafter.

5.3.2 Climate cooling

The long-term cooling trend through the middle and late Eocene, which was interrupted by the short-lived MECO warming event, does not explain the sudden radiolarian diversification in the late Eocene at Site 277. If gradual, long-term cooling was the driver of the expansion of high-latitude taxa, a progressive increase in such taxa would be expected over a longer time period. A gradual increase in high-latitude taxa is observed at Site 1172 from the middle Eocene but not at Site 277. Instead, the short-lived PrOM event appears to have been the trigger for the northward expansion of high-latitude taxa onto the Campbell Plateau. Whether this event was caused by an abrupt decline in atmospheric CO_2 concentrations or was related to the opening of the Tasmanian Gateway, which may have been open to surface circulation in early middle Eocene (Bijl et al., 2013), cannot be determined. Furthermore, astronomically induced changes also may have played a role. Laskar et al. (2004) calculated nodes in the amplitude modulation of eccentricity and obliquity at ∼ 37 Ma and Röhl et al. (2004) found evidence at Site 1172 for the increasing dominance of the 100 kyr eccentricity cycle at ∼ 37 Ma. Although there are nodes in amplitude modulation throughout the Eocene (Laskar et al, 2004), it is possible that a combination of these phenomena (e.g. a decrease in atmospheric CO_2, gateway opening and nodes in amplitude modulation) caused a cooling event. The amplitude modulation of obliquity, in particular, has been linked to climatic cooling in the Oligocene (Pälike et al., 2006).

The PrOM event at ∼ 37 Ma may have been associated with the formation of small Antarctic ice sheets (Scher et al., 2014), which in turn may have caused an intensification of currents in the Southern Ocean. Funakawa and Nishi (2008) reported a marked increase in radiolarian taxa with Antarctic faunal affinities at ODP Site 689 (Maud Rise, southern Atlantic) in the earliest late Eocene (∼ 38.6–36.9 Ma; Chron C17), which they interpreted to signify the northward expansion of the polar front that may be related to the PrOM. A subsequent decrease in Antarctic taxa, spanning chrons 16 and 15 (∼ 37–35 Ma), was related to the late Eocene warming event of Bohaty and Zachos (2003). These cooling and warming events appear to have caused longer-lived changes in radiolarian faunal assemblages than those observed at Site 277, lasting 1.7 and 2.0 Ma, respectively. This may reflect specific differences in the oceanographic settings of the two sites. Although the late Eocene warming event appears to be short-lived at Site 277, it may have spanned a longer interval of time elsewhere in the southwest Pacific. Incursions of warm-water foraminifera, including the low-latitude genus *Hantkenina*, are known to have occurred in the middle late Eocene (late Kaiatan–early Runangan) in sedimentary basins of southern New Zealand (Hornibrook et al., 1989; Hornibrook, 1992).

5.3.3 Radiolarian biogeographic reconstruction

During the middle Eocene, high-latitude radiolarian taxa were present at sites 277, 283, and 1172 (Fig. 7). The short-lived increase in abundance, diversity and the influx of low-latitude radiolarian *Amphicraspedum murrayanum* and *A. prolixum* gr. during the MECO at Site 277 and a high percentage of cosmopolitan taxa at Site 1172 suggest moderately warm temperatures at both sites, which may have been the result of a slightly stronger influence of an East Australian Current (EAC) (Fig. 8a). However, radiolarians and diatoms were abundant only at Site 1172 during the middle Eocene, which suggests a higher productivity region, perhaps a consequence of local of upwelling. The Tasmanian Gateway was open to a shallow westward-flowing Antarctic Slope Current (ASC), driven by the polar easterlies (Bijl et al., 2013; Scher et al., 2015).

During the onset of the PrOM event in the early late Eocene (~ 38–37 Ma, Fig. 8b), the abundance of high-latitude taxa increased at sites 1172 and 277. Additionally, sites 281 and 283 were characterised by high radiolarian abundance, with an average of ~ 61 and ~ 27 % high-latitude taxa, respectively. The region of high productivity expanded in this time, with the southernmost Site 281 having the highest D/R ratio in the interval (Fig. 8b). The region might have experienced an intensification of the Ross Gyre, extending the region of high productivity onto the Campbell Plateau and creating the Subtropical Front (STF) (Nelson and Cooke, 2001) (Fig. 8b).

During the late Eocene warming event (~ 36 Ma, Fig. 8c), radiolarian diversity decreased abruptly at Site 277, together with a decrease in high-latitude taxa (*Lithomelissa* spp., *Larcopyle* spp., Lophocyrtiidae; Table 2) and diatoms, and the appearance of low-latitude taxa at sites 283 and 277. Site 281 contains a late Eocene hiatus, implying an increase in the strength of bottom-water currents across the Tasmanian Gateway. We suggest that these changes were associated with a southward shift of the EAC that pushed the high-productivity zone of the STF towards the south, explaining the low radiolarian abundance and drop in diversity at Site 277. There is little evidence that the large Tasman Current as proposed by Huber et al. (2004) and Bijl et al. (2010) existed in the middle and late Eocene. Instead, our data suggest Site 277 was positioned at the northernmost limit of the influence of the Ross Gyre and the southernmost site of the influence of warm water delivered by the EAC.

During the latest Eocene–earliest Oligocene interval (~ 35–32 Ma, Fig. 8d), Site 277 experienced a second siliceous plankton bloom, associated with high radiolarian and diatom abundance and the reappearance of high-latitude taxa (Table 2). This suggests that latest Eocene cooling led to the expansion of the Ross Gyre to encroach on Campbell Plateau (Fig. 8d). At the same time, and perhaps reflecting strengthening of northward- and westward-flowing bottom currents, the area of non-deposition widened across the Tasmanian Gateway over sites 281, 283 and 1172. During the earliest Oligocene, the abundance of radiolarians and diatoms at Site 280 suggests a region of high primary productivity. This may have been a consequence of intensified upwelling associated with the ASC in conjunction with deepening in this sub-basin.

In contrast, diversity declines at Site 277 in the early Oligocene (Fig. 8e) and diatoms become scarce. The radiolarian fauna becomes dominated by *Lithelius minor* gr. and Actinommidae and many high-latitude taxa disappear (e.g. *Lithomelissa* spp., Table 2). This may be related to the development of the ACC. The ACC is inferred to have developed at ~ 30 Ma as the Tasmanian Gateway became fully open (Carter et al., 2004) and its northward expansion brought it in line with the westerly wind belt (Scher et al., 2015). This resulted in the zone of non-deposition extending over Site 280 as it moved into the path of the ACC. At Site 277, the radiolarian fauna is dominated by the high-latitude species *Axoprunum irregularis*, which is also dominant at Site 1172. Thus, the general low diversity of radiolarians and the scarcity of diatoms at Site 277 suggests the establishment of a cold-water nutrient-depleted environment, similar to the modern setting (Hollis and Neil, 2005). The development of the ACC restricted the northward extent of Ross Gyre and served to establish the Subantarctic Front on the southern margin of the Campbell Plateau (Carter et al., 2004).

6 Conclusions

Middle Eocene–early Oligocene radiolarian assemblages from DSDP sites 277, 280, 281, 283 and ODP Site 1172 were examined to investigate the relative influence of low- and high-latitude water masses in the southern southwest Pacific Ocean as global climate cooled and ice sheets expanded in Antarctica. In contrast to temperature reconstructions based on geochemical proxies that indicate subtropical–tropical temperatures at high latitudes during the middle and late Eocene (Liu et al., 2009; Bijl et al., 2010), Eocene radiolarian assemblages in this region lack significant numbers of warm-water taxa. Furthermore, we show that many high-latitude and taxa endemic to the Antarctic are already present in the middle Eocene. The MECO has been identified at Site 277 from foraminiferal δ^{18}O records and is associated with a short-lived incursion of two taxa with low-latitude affinities, *Amphicraspedum prolixum* gr. and *A. murrayanum*. The absence of definitive tropical taxa suggests warm temperate rather than tropical conditions during this short-lived event.

Radiolarians are very abundant and well preserved at high-latitude sites 281, 283 and 1172 during the early late Eocene and at Site 280 during the early Oligocene. For taxa with identified biogeographic affinities, those with high-latitude affinities comprise ~ 60 % at sites 280 and 281 and ~ 30 % at sites 283 and 1172. During the early late Eocene (~ 37 Ma), a positive shift in foraminiferal δ^{18}O values at Site 277 marks the onset of the PrOM event. A pronounced increase in diversity, abundance and preservation of radiolarians occurs in conjunction with this event at Site 277 in addition to a marked increase in diatom abundance. Many high-latitude taxa that are very abundant at sites 281 and 283 in the late middle Eocene and early late Eocene become abundant or have their LOs at Site 277 at ~ 37 Ma, including *Lithelius minor* gr., *Larcopyle hayesi*, *L. polyacantha*, *Spongopyle osculosa*, *Lithomelissa sphaerocephalis*, *L. gelasinus*, *L. ehrenbergi*, *Ceratocyrtis* spp., *Dictyophimus* aff. *archipilium*, *Lamprocyclas particollis*, and Antarctic morphotypes of *Aphetocyrtis gnomabax*, *A. rossi*, *Lophocyrtis aspera*, *L. keraspera* and *L. longiventer.* This northward extension of high-latitude taxa onto the Campbell Plateau appears to have been triggered by cooling during the PrOM event, which may have been associated with a short-lived development of an Antarctic ice sheet.

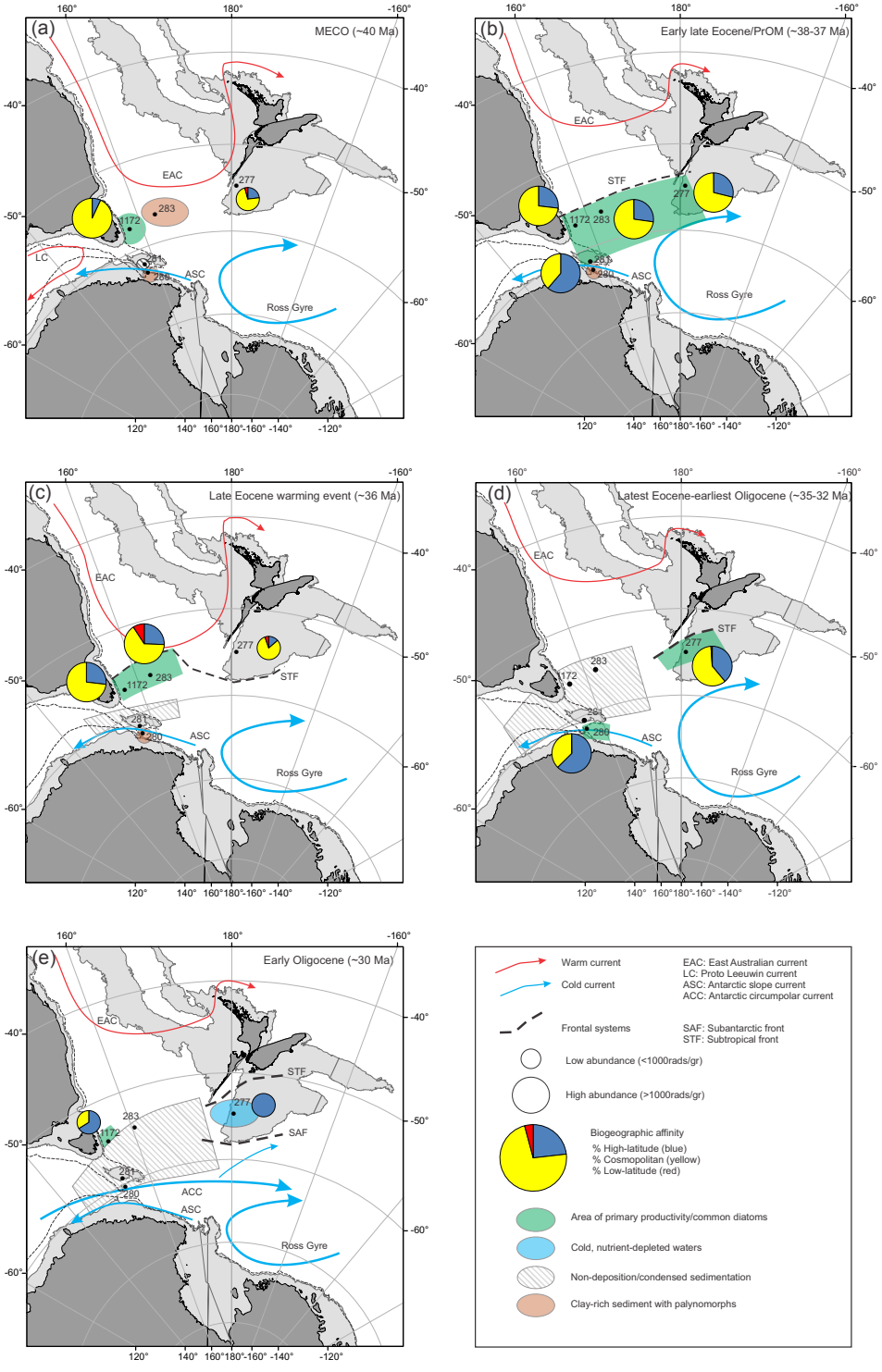

Figure 8. Palaeogeographic reconstructions and biogeographic affinities at investigated sites during the MECO (~ 40 Ma), early late Eocene/PrOM (~ 38–37 Ma), late Eocene warming event (~ 36 Ma), latest Eocene–earliest Oligocene (~ 35–32 Ma), and early Oligocene (~ 30 Ma). The 2000 m isobath from the GEBCO (www.gebco.net) bathymetric grid was used to approximate continental boundaries (light grey). The continental–oceanic boundaries of Bird (2003) are also shown for reference (dashed lines); continents with present-day shorelines are in dark grey. The late Eocene average is plotted for Site 1172 in map **(b)** and **(c)**.

A late Eocene warming event at ∼ 36 Ma is accompanied by a decrease in radiolarian diversity, high-latitude taxa and low diatom abundance at Site 277. Two low-latitude taxa, *Theocyrtis tuberosa* and *Thyrsocyrtis pinguisicoides*, make short-lived incursions into the southwest Pacific at this time. After this event, radiolarian diversity increases again with the reappearance of high-latitude taxa and abundant diatoms at Site 277. Through the EOT, radiolarians decrease in abundance and diversity at Site 277. Most nassellarian taxa within the Plagiacanthidae and Lophocyrtiidae decline, whereas *Lithelius minor* gr. and Actinommidae become dominant. Together with the scarcity of diatoms, we infer that conditions over the Campbell Plateau became nutrient-depleted as a consequence of the development of the ACC. The establishment of the ACC at around 30 Ma is inferred to have caused widespread non-deposition in the southwest Pacific and restricted the northward flow of Ross Gyre.

Acknowledgements. This study used bulk material and reference slides stored in the DSDP/ODP Micropaleontology Reference Centre, which is located at GNS Science, Lower Hutt, New Zealand. We greatly appreciate the reviews of David Lazarus and an anonymous referee, who provided helpful comments for improving our manuscript. We acknowledge the technical support of Sonja Bermudez (GNS Science), James Crampton (GNS Science) and Johan Renaudie (Museum für Naturkunde, Berlin) and editorial handling by Gerald Dickens. This project is funded by the New Zealand Marsden Fund (contract GNS1201).

Edited by: G. Dickens

References

Barron, J. A., Stickley, C. E., and Bukry, D.: Paleoceanographic, and paleoclimatic constraints on the global Eocene diatom and silicoflagellate record, Palaeogeogr. Palaeoclimatol. Palaeoecol., 422, 85–100, doi:10.1016/j.palaeo.2015.01.015, 2015.

Bijl, P. K., Houben, A. J., Schouten, S., Bohaty, S. M., Sluijs, A., Reichart, G.-J., Damsté, J. S. S., and Brinkhuis, H.: Transient Middle Eocene atmospheric CO2 and temperature variations, Science, 330, 819–821, 2010.

Bijl, P. K., Bendle, J. A., Bohaty, S. M., Pross, J., Schouten, S., Tauxe, L., Stickley, C. E., McKay, R. M., Röhl, U., and Olney, M.: Eocene cooling linked to early flow across the Tasmanian Gateway, P. Natl. Acad. Sci. USA, 110, 9645–9650, 2013.

Bird, P.: An updated digital model of plate boundaries, Geochem. Geophys. Geosyst., 4, 1027, doi:10.1029/2001GC000252, 2003.

Bohaty, S. M. and Zachos, J. C.: Significant Southern Ocean warming event in the late middle Eocene, Geology, 31, 1017–1020, doi:10.1130/G19800.1, 2003.

Bohaty, S. M., Zachos, J. C., Florindo, F., and Delaney, M. L.: Coupled greenhouse warming and deep-sea acidification in the middle Eocene, Paleoceanography, 24, PA2207, doi:10.1029/2008PA001676, 2009.

Bohaty, S. M., Zachos, J. C., and Delaney, M. L.: Foraminiferal Mg/Ca evidence for Southern Ocean cooling across the Eocene-Oligocene transition, Earth Planet. Sci. Lett., 317, 251–261, doi:10.1016/j.epsl.2011.11.037, 2012.

Boyden, J. A., Müller, R. D., Gurnis, M., Torsvik, T. H., Clark, J. A., Turner, M., Ivey-Law, H., Watson, R. J., and Cannon, J. S.: Next-generation plate-tectonic reconstructions using GPlates, Geoinformatics: cyberinfrastructure for the solid earth sciences, 95–114, 2011.

Cande, S. C. and Stock, J. M.: Pacific–Antarctic–Australia motion and the formation of the Macquarie Plate, Geophys. J. Int., 157, 399–414, 2004.

Carter, L., Carter, R., and McCave, I.: Evolution of the sedimentary system beneath the deep Pacific inflow off eastern New Zealand, Mar. Geol., 205, 9–27, 2004.

Casey, R. E.: Radiolaria, in: Fossil Prokaryotes and Protists, edited by: Lipps, J. H., Blackwell Scientific Publications, Oxford/London, UK, 249–284, 1993.

Caulet, J. P.: Radiolarians from the Kerguelen Plateau, Leg 119, edited by: Barron, J. A., Larsen, B. et al., Proceedings ODP, Scientific Results, 119, College Station, TX (Ocean Drilling Program), 513–546, doi:10.2973/odp.proc.sr.119.137.1991, 1991.

Chen, P. H.: Antarctic Radiolaria, in: Initial Reports of the Deep Sea Drilling Project, editd by: Hayes, D. E., Frakes, L. A., et al., Vol. 28, U.S. Government Printing Office, Washington, D.C., 437–513, doi:10.2973/dsdp.proc.28.111.1975, 1975.

Coxall, H. K., Wilson, P. A., Pälike, H., Lear, C. H., and Backman, J.: Rapid stepwise onset of Antarctic glaciation and deeper calcite compensation in the Pacific Ocean, Nature, 433, 53–57, 2005.

Croon, M. B., Cande, S. C., and Stock, J. M.: Revised Pacific-Antarctic plate motions and geophysics of the Menard Fracture Zone, Geochem. Geophys. Geosyst., 9, Q07001, doi:10.1029/2008GC002019, 2008.

Crouch, E. M. and Hollis, C. J.: Paleogene palynomorph and radiolarian biostratigraphy of DSDP Leg 29, sites 280 and 281 South Tasman Rise, Institute of Geological and Nuclear Sciences science report 96/19, 46 pp., 1996.

Diester-Haass, L. and Zahn, R.: Eocene-Oligocene transition in the Southern Ocean: History of water mass circulation and biological productivity, Geology, 24, 163–166, 1996.

Diester-Haass, L., Robert, C., and Chamley, H.: The Eocene-Oligocene preglacial-glacial transition in the Atlantic sector of the Southern Ocean (ODP Site 690), Mar. Geol., 131, 123–149, 1996.

Edwards, A. R. and Perch-Nielsen, K.: Calcareous nannofossils from the southern southwest Pacific, Deep Sea Drilling Project, Leg 29, edited by: Kennett, J. P., Houtz, R. E., et al., Initial Reports of the Deep Sea Drilling Project, Vol. 29, Washington, DC, US Government Printing Office, 469–539, doi:10.2973/dsdp.proc.29.113.1975, 1975.

Exon, N. F., Kennett, J. P., and Malone, M. J.: Leg 189 synthesis: Cretaceous-Holocene history of the Tasmanian gateway, Proceedings ODP, Scientific Results, 2004.

Florindo, F. and Roberts, A. P.: Eocene-Oligocene magnetobiochronology of ODP Sites 689 and 690, Maud Rise, Weddell Sea, Antarctica, Geol. Soc. Am. Bull., 117, 46–66, 2005.

Funakawa, S. and Nishi, H.: Late middle Eocene to late Oligocene radiolarian biostratigraphy in the Southern Ocean (Maud Rise, ODP Leg 113, Site 689), Mar. Micropaleontol., 54, 213–247, 2005.

Funakawa, S. and Nishi, H.: Radiolarian faunal changes during the Eocene-Oligocene transition in the Southern Ocean (Maud Rise, ODP Leg 113, Site 689) and its significance in paleoceanographic change, Micropaleontology, 54, 15–26, 2008.

Funakawa, S., Nishi, H., Moore, T. C., and Nigrini, C. A.: Radiolarian faunal turnover and paleoceanographic change around Eocene/Oligocene boundary in the central equatorial Pacific, ODP Leg 199, Holes 1218A, 1219A, and 1220A, Palaeogeogr. Palaeoclimatol. Palaeoecol., 230, 183–203, 2006.

Gradstein, F., Ogg, J., Schmitz, M., and Ogg, G.: The geologic time scale 2012, vol. 2, Elsevier New York, 2012.

Granot, R., Cande, S., Stock, J., and Damaske, D.: Revised Eocene-Oligocene kinematics for the West Antarctic rift system, Geophys. Res. Lett., 40, 279–284, doi:10.1029/2012GL054181, 2013.

Haeckel, E.: Report on the Radiolaria collected by H. M. S. Challenger during the years 1873–1876, Report on the Scientific Results of the Voyage of the H. M. S. Challenger, Zoology, 18, clxxxviii + 1803, 1887.

Hammer, Ø., Harper, D., and Ryan, P.: Past: Paleontological Statistics Software Package for education and data analysis, Paleontología Electrónica, 4, 1–9, available at: http://palaeo-electronica.org/2001_1/past/issue1_01.htm [download of version 3.07 on 24-07-2015, http://folk.uio.no/ohammer/past/], 2001.

Hill, D. J., Haywood, A. M., Valdes, P. J., Francis, J. E., Lunt, D. J., Wade, B. S., and Bowman, V. C.: Paleogeographic controls on the onset of the Antarctic circumpolar current, Geophys. Res. Lett., 40, 5199–5204, doi:10.1002/grl.50941, 2013.

Hollis, C. J.: Biostratigraphy and paleoceanographic significance of Paleocene radiolarians from offshore eastern New Zealand, Mar. Micropaleontol., 46, 265–316, 2002.

Hollis, C. J.: Radiolarian faunal change across the Paleocene-Eocene boundary at Mead Stream, New Zealand, Eclogae Geol. Helv., 99, S79–S99, 2006.

Hollis, C. and Neil, H.: Sedimentary record of radiolarian biogeography, offshore eastern New Zealand, New Zeal. J. Mar. Fresh., 39, 165–192, 2005.

Hollis, C. J., Waghorn, D. B., Strong, C. P., and Crouch, E. M.: Integrated Paleogene Biostratigraphy of DSDP Site 277 (Leg 29): Foraminifera, Calcareous Nannofossils, Radiolaria, and Palynomorphs, Institute of Geological & Nuclear Sciences Limited, 1997.

Hollis, C. J., Dickens, G. R., Field, B. D., Jones, C. M., and Percy Strong, C.: The Paleocene–Eocene transition at Mead Stream, New Zealand: a southern Pacific record of early Cenozoic global change, Palaeogeogr. Palaeoclimatol. Palaeoecol., 215, 313–343, 2005.

Hollis, C. J., Taylor, K. W. R., Handley, L., Pancost, R. D., Huber, M., Creech, J. B., Hines, B. R., Crouch, E. M., Morgans, H. E. G., Crampton, J. S., Gibbs, S., Pearson, P. N., and Zachos, J. C.: Early Paleogene temperature history of the Southwest Pacific Ocean: Reconciling proxies and models, Earth Planet. Sci. Lett., 349, 53–66, doi:10.1016/j.epsl.2012.06.024, 2012.

Hollis, C. J., Pascher, K. M., Hines, B. R., Littler, K., Kulhanek, D. K., Strong, C. P., Zachos, J. C., Eggins, S. M., and Philips, A.: Was the Early Eocene ocean unbearably warm or are the proxies unbelievably wrong?, Rendiconti Online, 31, 109–110, 2014.

Hornibrook, N. d. B.: New Zealand Cenozoic marine paleoclimates: a review based on the distribution of some shallow water and terrestrial biota, Pacific Neogene: environment, evolution, and events. University of Tokyo Press, Tokyo, 83–106, 1992.

Hornibrook, N. de B., Brazier, R. C., and Strong, C. P.: Manual of New Zealand Permian to Pleistocene foraminiferal biostratigraphy, Paleontological bulletin/New Zealand Geological Survey, 56, 1–175, 1989.

Houben, A. J., Bijl, P. K., Pross, J., Bohaty, S. M., Passchier, S., Stickley, C. E., Röhl, U., Sugisaki, S., Tauxe, L., and van de Flierdt, T.: Reorganization of Southern Ocean Plankton Ecosystem at the Onset of Antarctic Glaciation, Science, 340, 341–344, 2013.

Huber, M. and Sloan, L. C.: Heat transport, deep waters, and thermal gradients: Coupled simulation of an Eocene greenhouse climate, Geophys. Res. Lett., 28, 3481–3484, 2001.

Huber, M., Sloan, L. C., and Shellito, C.: Early Paleogene oceans and climate: A fully coupled modeling approach using the NCAR CCSM, Geological Society of America Special Papers, 369, 25–47, 2003.

Huber, M., Brinkhuis, H., Stickley, C. E., Döös, K., Sluijs, A., Warnaar, J., Schellenberg, S. A., and Williams, G. L.: Eocene circulation of the Southern Ocean: Was Antarctica kept warm by subtropical waters?, Paleoceanography, 19, PA4026, doi:10.1029/2004PA001014, 2004.

Jenkins, D. G.: Cenozoic planktic foraminiferal biostratigraphy of the southwestern Pacific and Tasman Sea – DSDP Leg 29, in: Initial Reports of the Deep Sea Drilling Project, edited by: Kennett, J. P., Houtz, R. E. et al., Vol. 29, U.S. Government Printing Office, Washington, D.C., 449–467, doi:10.2973/dsdp.proc.29.112.1975, 1975.

Kamikuri, S.-I., Moore, T. C., Lyle, M., Ogane, K., and Suzuki, N.: Early and Middle Eocene radiolarian assemblages in the eastern equatorial Pacific Ocean (IODP Leg 320 Site U1331): Faunal changes and implications for paleoceanography, Mar. Micropaleontol., 98, 1–13, doi:10.1016/j.marmicro.2012.09.004, 2013.

Katz, M. E., Miller, K. G., Wright, J. D., Wade, B. S., Browning, J. V., Cramer, B. S., and Rosenthal, Y.: Stepwise transition from the Eocene greenhouse to the Oligocene icehouse, Nature Geosci., 1, 329–334, 2008.

Keigwin, L.: Palaeoceanographic change in the Pacific at the Eocene-Oligocene boundary, Nature, 287, 722–725, 1980.

Keller, W. R.: Cenozoic plate tectonic reconstructions and plate boundary processes in the Southwest Pacific. Unpub. PhD Thesis: California Institute of Technology, Pasadena, 2003.

Kennett, J. P.: Cenozoic evolution of Antarctic glaciation, the circum-Antarctic Ocean, and their impact on global paleoceanography, J. Geophys. Res., 82, 3843–3860, 1977.

Kennett, J. P.: The development of planktonic biogeography in the Southern Ocean during the Cenozoic, Mar. Micropaleontol., 3, 301–345, 1978.

Kennett, J. P. and Exon, N. F.: Paleoceanographic evolution of the Tasmanian Seaway and its climatic implications, in: The Cenozoic Southern Ocean: Tectonics, Sedimentation, and Climate Change Between Australia and Antarctica, Geoph. Monog. Series, 151, 345–367, 2004.

Kennett, J. P., Houtz, R. E., Andrews, P. B., Edwards, A. R., Gostin, V. A., Hajós, M., Hampton, M., Jenkins, D. G., Margolis, S., Ovenshine, T., and Perch-Nielsen, K.: Initial Reports of the Deep

Sea Drilling Project, Vol. 29, U.S. Government Printing Office, Washington, D.C., 1975.

Laskar, J., Robutel, P., Joutel, F., Gastineau, M., Correia, A., and Levrard, B.: A long-term numerical solution for the insolation quantities of the Earth, Astron. Astrophys., 428, 261–285, 2004.

Lazarus, D.: Neptune: A marine micropaleontology database, Math. Geol., 26, 817–832, doi:10.1007/BF02083119, 1994.

Lazarus, D. and Caulet, J. P.: Cenozoic Southern Ocean reconstructions from sedimentologic, radiolarian, and other microfossil data, Antarct. Res. Ser., 60, 145–174, 1993.

Lazarus, D., Hollis, C., and Apel, M.: Patterns of opal and radiolarian change in the Antarctic mid-Paleogene: Clues to the origin of the Southern Ocean, Micropaleontology, 54, 41–48, 2008.

Liu, Z., Pagani, M., Zinniker, D., DeConto, R., Huber, M., Brinkhuis, H., Shah, S. R., Leckie, R. M., and Pearson, A.: Global cooling during the Eocene-Oligocene climate transition, Science, 323, 1187–1190, 2009.

Liu, J., Aitchison, J. C., and Ali, J. R.: Upper Paleocene radiolarians from DSDP Sites 549 and 550, Goban Spur, NE Atlantic, Palaeoworld, 20, 218–231, 2011.

Lunt, D. J., Dunkley Jones, T., Heinemann, M., Huber, M., LeGrande, A., Winguth, A., Loptson, C., Marotzke, J., Roberts, C. D., Tindall, J., Valdes, P., and Winguth, C.: A model-data comparison for a multi-model ensemble of early Eocene atmosphere-ocean simulations: EoMIP, Clim. Past, 8, 1717–1736, doi:10.5194/cp-8-1717-2012, 2012.

Morgans, H. E. G.: Late Paleocene to Middle Eocene foraminiferal biostratigraphy of the Hampden Beach section, eastern South Island, New Zealand, New Zeal. J. Geol. Geop., 52, 273–320, 2009.

Nelson, C. S. and Cooke, P. J.: History of oceanic front development in the New Zealand sector of the Southern Ocean during the Cenozoic – a synthesis, New Zeal. J. Geol. Geop., 44, 535–553, 2001.

O'Connor, B.: Stratigraphic and geographic distribution of Eocene Miocene Radiolaria from the southwest Pacific, Micropaleontology, 46, 189–228, 2000.

Pälike, H., Shackleton, N. J., and Röhl, U.: Astronomical forcing in Late Eocene marine sediments, Earth Planet. Sci. Lett., 193, 589–602, 2001.

Pälike, H., Frazier, J., and Zachos, J. C.: Extended orbitally forced palaeoclimatic records from the equatorial Atlantic Ceara Rise, Quaternary Sci. Rev., 25, 3138–3149, 2006.

Pearson, P. N., Ditchfield, P. W., Singano, J., Harcourt-Brown, K. G., Nicholas, C. J., Olsson, R. K., Shackleton, N. J., and Hall, M. A.: Warm tropical sea surface temperatures in the Late Cretaceous and Eocene epochs, Nature, 413, 481–487, 2001.

Petrushevskaya, M. G.: Cenozoic radiolarians of the Antarctic, Leg 29, DSDP, in: Initial Reports of the Deep Sea Drilling Project, edited by: Kennett, J. P., Houtz, R. E., et al., US Government Printing Office, Washington, DC, vol. 29, 541–675, doi:10.2973/dsdp.proc.29.114.1975, 1975.

Raine, J. I., Beu, A. G., Boyes, A. F., Campbell, H. J., Cooper, R. A., Crampton, J. S., Crundwell, M. P., Hollis, C. J., and Morgans, H. E. G.: Revised calibration of the New Zealand Geological Timescale : NZGT2015/1, Lower Hutt, N.Z.: GNS Science. GNS Science report 2012/3, 53 pp., 2015.

Röhl, U., Brinkhuis, H., Stickley, C. E., Fuller, M., Schellenberg, S. A., Wefer, G., and Williams, G. L.: Sea level and astronomically induced environmental changes in middle and late Eocene sediments from the East Tasman Plateau, in: The Cenozoic Southern Ocean: tectonics, sedimentation, and climate change between Australia and Antarctica, edited by: Exon, N. F., Kennett, J. P., and Malone, M. J., Am. Geophys. Union, Geophys. Monogr., 151, 127–151, 2004.

Sanfilippo, A. and Caulet, J. P.: Taxonomy and evolution of Paleogene Antartic and Tropical Lophocyrtid radiolarians, Micropaleontology, 44, 1–43, 1998.

Sanfilippo, A., Westberg-Smith, M. J., and Riedel, W. R.: Cenozoic radiolaria, in: Plankton stratigraphy: Volume 2, Radiolaria, Diatoms, Silicoflagellates, Dinoflagellates and Ichthyoliths, edited by: Bolli, H. M., Saunders, J. B., and Perch-Nielsen, K., 631–712, 1985.

Scher, H. D., Bohaty, S. M., Smith, B. W., and Munn, G. H.: Isotopic interrogation of a suspected late Eocene glaciation, Paleoceanography, 29, 2014PA002648, doi:10.1002/2014PA002648, 2014.

Scher, H. D., Whittaker, J. M., Williams, S. E., Latimer, J. C., Kordesch, W. E., and Delaney, M. L.: Onset of Antarctic Circumpolar Current 30 million years ago as Tasmanian Gateway aligned with westerlies, Nature, 523, 580–583, 2015.

Sexton, P. F., Wilson, P. A., and Norris, R. D.: Testing the Cenozoic multisite composite delta(18)O and delta(13)C curves: New monospecific Eocene records from a single locality, Demerara Rise (Ocean Drilling Program Leg 207), Paleoceanography, 21, PA2019, doi:10.1029/2005PA001253, 2006.

Shackleton, N. and Kennett, J.: Paleotemperature history of the Cenozoic and the initiation of Antarctic glaciation: oxygen and carbon isotope analyses in DSDP Sites 277, 279, and 281, in: Kennett, J. P., Houtz, R. E., et al., Initial reports of the deep sea drilling project, Vol. 29, 743–755, doi:10.2973/dsdp.proc.29.117.1975, 1975.

Spencer-Cervato, C.: The Cenozoic deep sea microfossil record: explorations of the DSDP/ODP sample set using the Neptune database, Palaeontologia Electronica, 2, 270, 1999.

Spiess, V.: Cenozoic magnetostratigraphy of Leg 113 drill sites, Maud Rise, Weddell Sea, Antarctica, Proceedings ODP, Scientific Results, 113, Ocean Drilling Program, College Station, TX, 261–315, doi:10.2973/odp.proc.sr.113.182.1990, 1990.

Stickley, C. E., Brinkhuis, H., Schellenberg, S. A., Sluijs, A., Röhl, U., Fuller, M., Grauert, M., Huber, M., Warnaar, J., and Williams, G. L.: Timing and nature of the deepening of the Tasmanian Gateway, Paleoceanography, 19, PA4027, doi:10.1029/2004PA001022, 2004.

Sutherland, R.: The Australia-Pacific boundary and Cenozoic plate motions in the SW Pacific: Some constraints from Geosat data, Tectonics, 14, 819–831, 1995.

Suzuki, N., Ogane, K., and Chiba, K.: Middle to Late Eocene polycystine radiolarians from the Site 1172, Leg 189, Southwest Pacific, News of Osaka Micropaleontologists, special volume, 14, 239–296, 2009.

Takemura, A.: Radiolarian Paleogene biostratigraphy in the southern Indian Ocean, Leg 120, edited by: Wise Jr., S. W., Schlich, R. et al., Proceedings ODP, Scientific Results, 120, Ocean Drilling Program, College Station, TX, 735–756, doi:10.2973.odp.proc.sr.120.177, 1992.

Takemura, A. and Ling, H. Y.: Eocene and Oligocene radiolarian biostratigraphy from the Southern Ocean – correlation of ODP

Legs 114 (Atlantic Ocean) and 120 (Indian Ocean), Mar. Micropaleontol., 30, 97–116, 1997.

Torsvik, T. H., Van der Voo, R., Preeden, U., Mac Niocaill, C., Steinberger, B., Doubrovine, P. V., van Hinsbergen, D. J., Domeier, M., Gaina, C., and Tohver, E.: Phanerozoic polar wander, palaeogeography and dynamics, Earth Sci. Rev., 114, 325–368, 2012.

van Hinsbergen, D. J., de Groot, L. V., van Schaik, S. J., Spakman, W., Bijl, P. K., Sluijs, A., Langereis, C. G., and Brinkhuis, H.: A Paleolatitude Calculator for Paleoclimate Studies, PloS one, 10, e0126946, doi:10.1371/journal.pone.0126946, 2015.

Villa, G., Fioroni, C., Pea, L., Bohaty, S., and Persico, D.: Middle Eocene–late Oligocene climate variability: calcareous nannofossil response at Kerguelen Plateau, Site 748, Mar. Micropaleontol., 69, 173–192, 2008.

Villa, G., Fioroni, C., Persico, D., Roberts, A. P., and Florindo, F.: Middle Eocene to Late Oligocene Antarctic glaciation/deglaciation and Southern Ocean productivity, Paleoceanography, 29, 2013PA002518, doi:10.1002/2013PA002518, 2014.

Vonhof, H. B., Smit, J., Brinkhuis, H., Montanari, A., and Nederbragt, A. J.: Global cooling accelerated by early late Eocene impacts?, Geology, 28, 687–690, 2000.

Westerhold, T., Röhl, U., Pälike, H., Wilkens, R., Wilson, P. A., and Acton, G.: Orbitally tuned timescale and astronomical forcing in the middle Eocene to early Oligocene, Clim. Past, 10, 955–973, doi:10.5194/cp-10-955-2014, 2014.

Zachos, J. C., Quinn, T. M., and Salamy, K. A.: High-resolution (104 years) deep-sea foraminiferal stable isotope records of the Eocene-Oligocene climate transition, Paleoceanography, 11, 251–266, 1996.

Zachos, J. C., Pagani, M., Sloan, L., Thomas, E., and Billups, K.: Trends, rhythms, and aberrations in global climate 65 Ma to present, Science, 292, 686–693, 2001.